Forced baroclinic ocean motions, III: The linear equatorial basin case

by Mark A. Cane[1] and E. S. Sarachik[2]

ABSTRACT

Previous work on the linear spin-up of an equatorial ocean is extended to include the specific effects of the north-south extent of the basin, thus allowing a detailed comparison of analytic spin-up theory with numerical calculations.

North-south modes in a β-plane equatorial basin are solved for both numerically and analytically. Simple approximations are developed and the modes are classified by the location of the turning points relative to the zonal walls. The modes are illustrated for three cases: A: a symmetric basin whose zonal walls are distant from the equator (compared to the equatorial radius of deformation); B: a symmetric basin whose zonal walls are close to the equator; and C: an asymmetric basin, one wall of which is close to the equator and one far.

Spin-up in response to x-independent winds in each of these basins is then calculated in terms of four elements: the x-independent response to the wind; the eastern boundary response consisting of Rossby and Rossby-Kelvin modes needed to bring the u field to zero; the western boundary response consisting of Kelvin waves needed to bring the u field to zero; and the western boundary layer consisting of trapped short Rossby waves needed to bring u to zero and meridionally redistribute mass. These elements are combined to describe how the steady (Sverdrup) solutions are approached. Special attention is paid to the fast planetary response: the equatorially confined Kelvin mode, the exponential anti-Kelvin mode with maximum amplitude on the zonal walls, and the Rossby-Kelvin mode, the latter two being modes not present on a meridionally open basin.

Finally, a numerical model is run to illustrate spin-up for various winds in each of the basins, A, B and C.

1. Introduction

This paper is the third of a series describing the linear response to simple wind stress patterns of an equatorial ocean described by the baroclinic shallow water equations.

In the first paper (Cane and Sarachik, 1976, henceforth called I), we described

1. Laboratory for Atmospheric Sciences, NASA Goddard Space Flight Center, Greenbelt, Maryland, 20770, U.S.A.

2. Center for Earth and Planetary Physics, Harvard University, Cambridge, Massachusetts, 02138, U.S.A.

the response of an unbounded equatorial ocean to zonal and meridional wind stresses switched on in time and space. The dispersive properties of these forced wave motions were clarified by investigating the dispersive properties of a closely analogous system: the barotropic vorticity equation forced by a switched on wind stress curl. It was found that the asymptotic westward response occurred behind fronts propagating with the long Rossby nondispersive wave speed; and that asymptotic eastward motions occurred only at forcing discontinuities or western boundaries and consisted of short Rossby waves in the form of Bessel function "Gulf Streams" rapidly thinning with time. These results extend directly to the planetary wave part of the baroclinic case, this case being completed by the addition of eastward responses behind fronts travelling with the Kelvin wave speed. A method, based on the one of Matsuno (1966), was then introduced for calculating the unbounded baroclinic response, and this unbounded response was calculated for several unbounded zonal and meridional wind stresses. It was found that, in general, zonal winds excite a local resonant response that has the u and h fields growing linearly with time and the v field constant with time. By contrast, a meridional wind excites local u and h fields constant in time with no steady v field at all. The role of the equatorial inertia-gravity waves in setting up these unbounded responses was elucidated.

In the second paper (Cane and Sarachik, 1977, henceforth called II), we considered the effects of meridional boundaries at $x = 0$ and $x = X_E$ and described the spin-up of this zonally bounded but meridionally unbounded equatorial ocean. The method consisted of three basic steps: (i) the calculation of the fully unbounded response, as given in I; (ii) the calculation of the boundary responses needed to bring the zonal velocity of the unbounded response to zero on the boundaries; and (iii) the calculation of the boundary reflections necessary to bring to zero the zonal velocities of any of the wave responses calculated in step (ii) and any of their subsequent reflections. These boundary reflections in steps (ii) and (iii) were calculated by a method due to Moore (Moore and Philander, 1977). The method depends in an essential way on the detailed properties of the Hermite functions, which are the correct functions to use only when the basin is meridionally unbounded. The motions excited by switched on wind stresses were followed in time and the precise manner in which the wave motions conspired to produce the steady (Sverdrup) solution was studied. It was found that the approach to the steady solution is significantly impeded when Kelvin waves are excited, for these Kelvin waves induce a sloshing of mass back and forth across the basin with only slowly decreasing amplitude. It was argued in this paper that despite the unrealistic unboundedness of the basin in the meridional direction, the results obtained should be valid in the vicinity of the equator.

It is the purpose of this paper to explicitly include the boundedness of the basin in the meridional direction in the description of the spin-up process and in so doing

to decide if any essential features are introduced by these boundaries at the north and south. Thus we will solve the non-dimensional shallow water equations

$$u_t - yv + h_x = F\,H(t) \tag{1a}$$

$$v_t + yu + h_y = G\,H(t) \tag{1b}$$

$$h_t + u_x + v_y = Q\,H(t) \tag{1c}$$

subject to the boundary conditions

$$u = 0 \text{ at } x = 0 \text{ and } X_E \tag{2a}$$

$$v = 0 \text{ at } y = Y_S \text{ and } Y_N \tag{2b}$$

where in general Y_S will be taken to be south of the equator and Y_N will be taken to be north.

The imposition of meridional boundedness in condition (2b) means that the meridional eigenmodes will no longer simply be related to the Hermite functions. Hickie (1979) solved for the eigenvalues and eigenfunctions of a basin bounded in one meridional direction and found that the deviation from the Hermite-like behavior increased as the boundary approached the equator. As we will see, Hickie's assumption of unboundedness in one direction eliminates some important solutions (we will call them anti-Kelvin waves) that were previously noted by Moore (1968) and Mofjeld and Rattray (1971) in their discussions of free modes of an equatorial basin.

In what follows, the basic method of calculating the time dependent response is essentially the same as the method of II and can be summarized by noting the equivalent 3-step process: (i) the zonally unbounded, but meridionally bounded, response is calculated; (ii) the eastern and western boundary response needed to bring to zero the zonal velocity field of the zonally unbounded response of step (i) is calculated; (iii) the eastern and western boundary response needed to bring to zero the zonal velocity fields of any boundary responses emitted subsequently as part of step (ii) is calculated. It should be noted that the inclusion of northern and southern boundaries complicates the analytic problem significantly, yet resolution of this complication is essential before analytic results can be compared to, say, numerical simulations.

The plan of this paper is as follows: the second section will describe the eigenvalues and eigenfunctions of the v equation in a meridionally bounded domain. Analytic approximations are compared in detail with numerically generated results. Special emphasis is placed on modes not present in the meridionally unbounded case, in particular the westward propagating Rossby-Kelvin, anti-Kelvin and inertia-Kelvin modes, all of which have large amplitude at the zonal boundaries.

The third section reviews notation for the vector eigenfunctions, describes their completeness and orthogonality properties, and uses them to implement step (i),

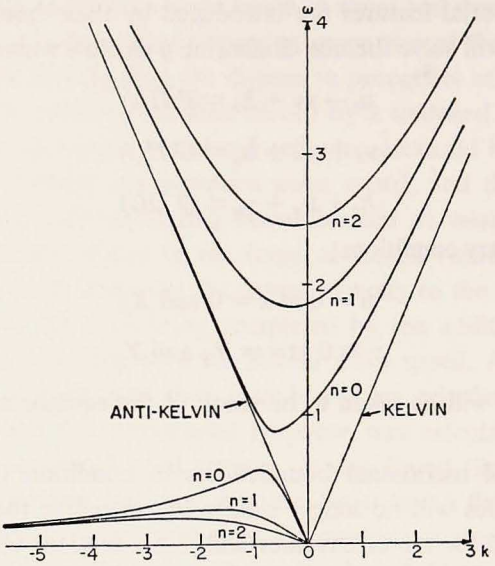

Figure 1. The dispersion relation (Eq. (5)) drawn for the eigenvalues of the [−5,1.7] case. The $n = 0$ low frequency branch is the Kelvin-Rossby mode; the $n = 0$ high frequency branch is the inertia-Kelvin mode.

the calculation of the meridionally bounded but zonally unbounded response. The fourth section shows how to calculate the eastern and western boundary response and thus how to implement steps (ii) and (iii) described above.

Section 5 will describe in some detail the time dependent response of three equatorial basins to $F = 1$ and $G = 1$ wind stresses. This will be done by presenting a linear numerical simulation of the spin-up process and comparing with the linear analytic theory developed in the earlier sections. Finally, the applicability and limits of this work to the baroclinic response of real equatorial oceans will be discussed in the last section, and our conclusions will be given.

2. The free modes of the meridional velocity equation

The homogeneous set of equations (1) with $F = G = Q = 0$ and dependence $u, v, h \sim e^{i(kx-\omega t)}$ can be reduced to a single equation for v:

$$v_{yy} + [2\mu + 1 - y^2]\, v = 0 \tag{3}$$

subject to the conditions at the northern and southern boundaries

$$v = 0 \text{ at } Y_S, Y_N\,. \tag{4}$$

In terms of the eigenvalues μ_n, the nondimensional dispersion relation is

$$\omega_n{}^2 - k^2 - \frac{k}{\omega_n} = 2\mu_n + 1\,. \tag{5}$$

There are two linearly independent solutions to (3) so that the general solution of (3) may be written, in the notation of Abramowitz and Stegun (1965):

$$v(y) = U(-\mu - 1/2, \sqrt{2}\, y) + bV(-\mu - 1/2, \sqrt{2}\, y) \tag{6}$$

where $U(V)$ is the parabolic cylinder function that decays (blows up) exponentially as $y \to +\infty$.

We will take Y_N to be north of the equator and Y_S to be south so that applying the boundary condition (4) at the northern boundary yields

$$b = -\frac{U(-\mu - 1/2, \sqrt{2}\, Y_N)}{V(-\mu - 1/2, \sqrt{2}\, Y_N)}. \tag{7a}$$

Applying the boundary condition at the southern boundary yields an eigenvalue equation for the sequence of eigenvalues μ_n:

$$U(-\mu_n - 1/2, -\sqrt{2}\,|Y_S|) - \frac{U(-\mu_n - 1/2, \sqrt{2}\, Y_N)}{V(-\mu_n - 1/2, \sqrt{2}\, Y_N)} V(-\mu_n - 1/2, -\sqrt{2}\,|Y_S|) = 0. \tag{7b}$$

Since Equation (3) with boundary conditions (4) is of standard Sturm-Liouville form, we may immediately conclude that the eigenvalues form a nonnegative increasing sequence and that the eigenfunctions are complete and orthogonal on the interval $[Y_S, Y_N]$.

Equations (6), (7a) and (7b) give the general solution to the problem, but since the content of these equations is at best opaque we will examine various approximations to the solutions with a view toward deriving analytic approximations for the eigenvalues and eigenfunctions and thus understanding them in simpler terms.

To begin with, we must recognize that the solutions U and V have Stokes lines in the complex plane so that analytic continuation across these lines changes the form of the representation. Since we will need only the representation of the solution for real positive and negative values of y, we will need only the auxiliary relations (Abramowitz and Stegun, 1965)

$$U(-\mu - 1/2, -y) = \frac{\pi V(-\mu - 1/2, y)}{\Gamma(-\mu)} + \cos \pi\mu\, U(-\mu - 1/2, y) \tag{8a}$$

and

$$V(-\mu - 1/2, -y) = (1/\pi) \sin^2 \pi\mu\, \Gamma(-\mu)\; U(-\mu - 1/2, y) - \cos \pi\mu\, V(-\mu - 1/2, y) \tag{8b}$$

both valid for $y > 0$. Using these relations in (7b), the eigenvalue equation can be written in terms of $U(y)$ and $V(y)$ with positive argument only:

$$\frac{\pi}{\Gamma(-\mu_n)\cos\pi\mu_n} + \frac{U(-\mu_n - 1/2, \sqrt{2}\,|Y_S|)}{V(-\mu_n - 1/2, \sqrt{2}\,|Y_S|)}$$

$$+ b_n\left[\frac{\sin^2\pi\mu_n}{\pi\cos\pi\mu_n}\,\Gamma(-\mu_n)\,\frac{U(-\mu_n - 1/2, \sqrt{2}\,|Y_S|)}{V(-\mu_n - 1/2, \sqrt{2}\,|Y_S|)} - 1\right] = 0$$

where b_n is given by (7a) when μ takes on one of the eigenvalues μ_n. Simplifying using the standard relation

$$\Gamma(-\mu)\,\Gamma(\mu + 1)\sin\pi\mu = -\pi \tag{9}$$

yields

$$\Gamma(\mu_n + 1)\tan\pi\mu_n - \frac{U(-\mu_n - 1/2, \sqrt{2}\,|Y_S|)}{V(-\mu_n - 1/2, \sqrt{2}\,|Y_S|)}$$

$$+ b_n\left[\frac{\cot\pi\mu_n}{\Gamma(\mu_n + 1)}\,\frac{U(-\mu_n - 1/2, \sqrt{2}\,|Y_S|)}{V(-\mu_n - 1/2, \sqrt{2}\,|Y_S|)} + 1\right] = 0\,. \tag{10}$$

In the limit that $Y_N \to \infty$, $b_n \to 0$, and using (8a), the eigenvalue equation reduces to that of Hickie (1979):

$$U(-\mu_n - 1/2, \sqrt{2}\,Y_S) = 0 \tag{11a}$$

recalling that Y_S is negative. In the opposite limit that $Y_S \to -\infty$, (10) reduces to $b_n + \Gamma(\mu_n + 1)\tan\pi\mu_n = 0$, or, again using (8a)

$$U(-\mu_n - 1/2, -\sqrt{2}\,Y_N) = 0\,. \tag{11b}$$

In the limit that both $Y_N \to +\infty$ and $Y_S \to -\infty$, (10) reduces to $\Gamma(\mu_n + 1) \cdot \tan\pi\mu_n = 0$, i.e., $\mu_n = n$ where n is a nonnegative integer. This limit represents the meridionally unbounded case treated in Papers I and II: the functions V never appear and $U(-n - 1/2, \sqrt{2}\,y)$ are simply the Hermite functions $H_n(y)\exp[-y^2/2]$ treated previously.

For the meridionally bounded case, (10) represents the general eigenvalue equation and can be solved in various analytic approximations. These approximations can be classified by the location with respect to the northern and southern boundaries of the turning points of the nth eigenfunction at $y = \pm\sqrt{2\mu_n + 1}$.

There are four cases of interest:

(i) Both turning points lie well within the basin, i.e., $2\mu_n + 1 << Y_S^2$ and Y_N^2.

Using the asymptotic forms valid for $y^2 >> 2\mu + 1$,

$$U(-\mu - 1/2, y) \to y^\mu \exp[-y^2/4]$$

$$V(-\mu - 1/2, y) \to \sqrt{2/\pi}\,(y)^{-\mu-1}\exp[+y^2/4] \tag{12}$$

gives

$$b_n = -\sqrt{\pi/2}\,(\sqrt{2}\,Y_N)^{2\mu_n+1}\quad e^{-Y_N^2} \tag{13}$$

and the approximate eigenvalue equation

$$\Gamma(\mu_n+1)\tan\pi\mu_n = \sqrt{\pi/2}\left[(\sqrt{2}\,|Y_S|)^{2\mu_n+1}\quad e^{-Y_S^2} + (\sqrt{2}\,Y_N)^{2\mu_n+1}\quad e^{-Y_N^2}\right]. \tag{14}$$

Since the right-hand side of (14) is small, the eigenvalues are approximately integer and Eq. (14) can be solved approximately to yield

$$\mu_n \approx n + (2\pi)^{-1/2}\,(n!)^{-1}\left[\,(\sqrt{2}\,|Y_S|)^{2n+1}\,e^{-Y_S^2} + (\sqrt{2}\,Y_N)^{2n+1}\,e^{-Y_N^2}\,\right]. \tag{15}$$

The eigenfunctions are oscillatory between the turning points and decaying beyond.

(ii) The northern turning point lies well within the basin but the southern one lies well outside the basin, i.e., $Y_S^2 << 2\mu_n + 1 << Y_N^2$.

The asymptotic relations (12) are again used to give the same b_n as in (13). But for $y^2 << 2\mu_n + 1$

$$\frac{U(-\mu_n - 1/2,\, y)}{V(-\mu_n - 1/2,\, y)} \to \Gamma(\mu_n+1)\cot\Phi_n(y) \tag{16}$$

where, to third order in $y(2\mu_n+1)^{-1/2}$,

$$\Phi_n(y) = (\mu_n + 1/2)^{1/2}\,y - (\pi/2)\,\mu_n - (1/24)\,y^3\,(\mu_n+1/2)^{-1/2}.$$

The eigenvalue Eq. (10) becomes, approximately,

$$\tan\pi\mu_n = \cot\Phi_n\,(\sqrt{2}\,|Y_S|) + \sqrt{\pi/2}\,\frac{(\sqrt{2}\,Y_N)^{2\mu_n+1}\quad e^{-Y_N^2}}{\Gamma(\mu_n+1)}\,[\tan\pi\mu_n\cot\Phi_n\,(\sqrt{2}\,|Y_S|)+1]. \tag{17}$$

An explicit solution to (17) is reached by first solving

$$\tan\pi\mu_n^{(0)} = \cot\left[(2\mu_n^{(0)}+1)^{1/2}\,|Y_S| - (\pi/2)\,\mu_n^{(0)} - (1/6)\,|Y_S|^3\,(2\mu_n^{(0)}+1)^{-1/2}\right] \tag{18}$$

for $\mu_n^{(0)}$. (Note that $\mu_n^{(0)}$ is the eigenvalue when $Y_N \to +\infty$.)

The approximate solutions to (17) are then

$$\mu_n = \mu_n^{(0)} + \sqrt{2/\pi}\,\frac{(\sqrt{2}\,Y_N)^{2\mu_n^{(0)}+1}}{\Gamma(\mu_n^{(0)}+1)}\quad e^{-Y_N^2} \tag{19}$$

$$\cdot \left[1 + (2/\pi) \frac{Y_N}{(2\mu_n{}^{(0)} + 1)^{1/2}} - \frac{1}{3\pi} \frac{Y_N{}^3}{(2\mu_n{}^{(0)} + 1)^{3/2}} \right]^{-1} \cdot$$

The eigenfunctions are oscillatory from Y_S to the turning point and decaying further northward.

(iii) The southern turning point lies well within the basin but the northern one lies well outside the basin, i.e., $Y_N{}^2 << 2\mu_n + 1 << Y_S{}^2$.

Now

$$b_n = -\Gamma(\mu_n + 1) \cot \Phi_n (\sqrt{2}\, Y_N),$$

while

$$\tan \pi\mu_n = \cot \Phi(\sqrt{2}\, Y_N)$$

$$+ \sqrt{\pi/2} \frac{(\sqrt{2}\,|Y_S|)^{2\mu_n+1}\ e^{-Y_S{}^2}}{\Gamma(\mu_n + 1)} \left[\tan \pi\mu_n \cot \Phi_n(\sqrt{2}\, Y_N) + 1\right].$$

Again the equation

$$\tan \mu_n{}^{(0)} = \cot \left[(2\mu_n{}^{(0)} + 1)^{1/2} Y_N - (\pi/2)\, \mu_n{}^{(0)} - (1/6)\, Y_N{}^3 (2\mu_n{}^{(0)} + 1)^{-1/2}\right] \tag{20a}$$

is solved and the approximate eigenvalues are

$$\mu_n = \mu_n{}^{(0)} + \sqrt{2/\pi} \frac{(\sqrt{2}\,|Y_S|^{2\mu_n{}^{(0)}+1}}{\Gamma(\mu_n{}^{(0)} + 1)} \tag{20b}$$

$$\cdot e^{-Y_S{}^2} \left[1 + (2/\pi) \frac{|Y_S|}{(2\mu_n{}^{(0)} + 1)^{1/2}} - \frac{1}{3\pi} \frac{|Y_S|^3}{(2\mu_n{}^{(0)} + 1)^{3/2}} \right]^{-1}$$

The eigenfunctions are decaying south of the turning point and oscillatory from the turning point to Y_N.

(iv) Both turning points lie well outside the basin, i.e., $Y_S{}^2$ and $Y_N{}^2 << 2\mu_n + 1$.

Only the asymptotic relation (16) need be used for this case. We find

$$b_n = -\Gamma(\mu_n + 1) \cot \Phi_n (\sqrt{2}\, Y_N) \tag{21}$$

and the eigenvalue Eq. (10) reduces simply to

$$\sin \left[(2\mu_n + 1)^{1/2} (|Y_S| + Y_N) - (1/6)\, (2\mu_n + 1)^{-1/2} \cdot (|Y_S|^3 + Y_N{}^3)\right] = 0 \tag{22}$$

with solution, valid to $0(1/n^2)$,

$$\mu_{n-1} = (1/2) \left\{ \frac{n^2\pi^2}{(|Y_S| + Y_N)^2} + (1/3) \frac{|Y_S|^3 + Y_N{}^3}{|Y_S| + Y_N} - 1 - \frac{(|Y_S|^3 + Y_N{}^3)^2}{36n^2\pi^2} \right\}, \qquad n = 1, 2, 3, \ldots . \tag{23}$$

The solution (22) and (23), to order n^2, is identical to the solution of the equations of motions without any coriolis force at all in a meridionally bounded basin; the corresponding eigenfunctions are just sines. The additional terms to 0(1) and $0(1/n^2)$ are significant corrections for the low order modes but lose their importance for the higher modes.

Finally, we note that for $2\mu_n + 1$ large (it need be no smaller than 10), there is a *uniform* approximation for the solutions of (3) (Abramowitz and Stegun, 1965)

$$U(-\mu - 1/2, y) = 2^{\mu/2}\,\Gamma\left(\frac{\mu+1}{2}\right)\left(\frac{t}{\xi^2-1}\right)^{1/4} Ai(t) \tag{24a}$$

and

$$\Gamma(\mu+1)\,V(-\mu-1/2, y) = 2^{\mu/2}\,\Gamma\left(\frac{\mu+1}{2}\right)\left(\frac{t}{\xi^2-1}\right)^{1/4} Bi(t) \tag{24b}$$

where

$$\xi = y(2\mu+1)^{-1/2},\ t = (4\mu+2)^{2/3}\,\tau$$

and

$$\tau = -\left(\frac{3}{2}\ \theta_3\right)^{2/3} \qquad \xi \leqslant 1\,,$$

$$\tau = \left(\frac{3}{2}\ \theta_2\right)^{2/3} \qquad \xi \geqslant 1$$

with

$$\theta_3 = (1/4)\ \arccos \xi - (1/4)\,\xi\sqrt{1-\xi^2}$$

$$\theta_2 = (1/4)\,\xi\sqrt{\xi^2-1} - (1/4)\ \operatorname{arccosh} \xi\,.$$

(7a) and (10) then become

$$b_n = -\,\Gamma(\mu_n+1)\,\frac{Ai[t_n(\sqrt{2}\,Y_N)]}{Bi[t_n(\sqrt{2}\,Y_N)]} \tag{25}$$

and

$$\tan \pi\mu_n\left[\,1 - \frac{Ai[t_n(\sqrt{2}\,Y_N)]\,Ai[t_n(\sqrt{2}\,|Y_S|)]}{Bi[t_n(\sqrt{2}\,Y_N)]\,Bi[t_n(\sqrt{2}\,|Y_S|)]}\right] - \left[\frac{Ai[t_n(\sqrt{2}\,|Y_S|)]}{Bi[t_n(\sqrt{2}\,|Y_S|)]}\right] - \left[\frac{Ai[t_n(\sqrt{2}\,Y_N)]}{Bi[t_n(\sqrt{2}\,Y_N)]}\right] = 0\,. \tag{26}$$

It can be checked, by using the appropriate asymptotics of the Airy functions, that cases (i), (ii), (iii) and (iv) can be derived as the appropriate low order limits of (25) and (26).

We will illustrate these results by comparing these analytic approximations with

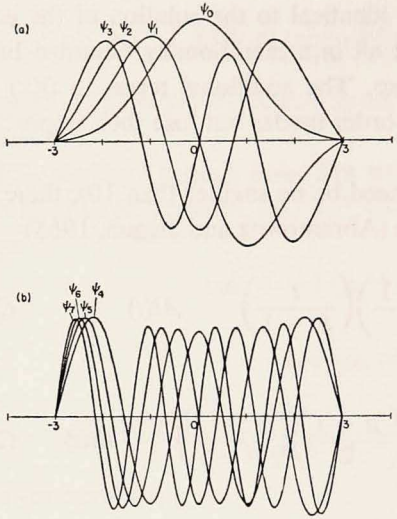

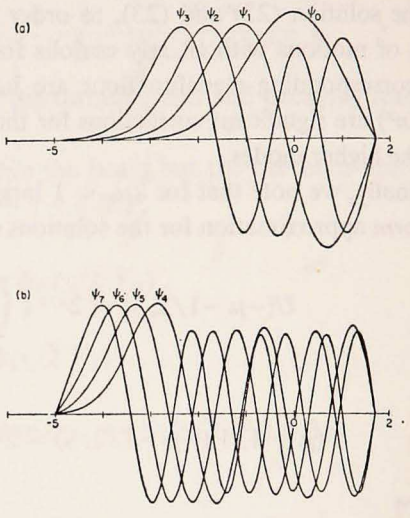

Figure 2. (left). Normalized eigenmodes of the v equation (3) for a [−3,3] basin. (a) Modes $n = 0$ to 3; (b) Modes $n = 4$ to 7.

Figure 3. (right). Normalized eigenmodes of the v equation (3) for an asymmetric [−5,1.7] basin. (a) Modes $n = 0$ to 3; (b) Modes $n = 4$ to 7.

results obtained by solving (3) and (4) by direct numerical means. We will consider three separate basins, one basin symmetric about the equator whose walls are relatively far from the equator, [−3,3], one asymmetric basin whose northern wall is relatively close to the equator at approximately the same position as the Gulf of Guinea, [−5,1.7], and a symmetric basin both of whose walls are close to the equator, [−1.7,1.7].

a. Basin [−3,3]

The first eight eigenfunctions are shown in Figure 2. The first four have $\sqrt{2\mu + 1} < 3$ so their turning points are inside the basin. In each of these first four eigenfunctions we see evidence of decay toward the northern and southern boundaries with oscillatory behavior equatorward of this decay. Starting with the fifth eigenfunction, the turning points are outside the basin and no evidence of decay toward the walls is seen. In accordance with the properties of the Airy and Bairy functions in (24), we notice that the envelope of the oscillatory part of the eigenfunctions decays toward the equator.

We can compare the numerically obtained eigenvalue with the two approximations relevant to this case—(i) and (iv).

The approximation (15) for the lowest two eigenvalues is quite good because the exponential decay of the eigenfunction toward the walls is quite rapid. The approximation (23) is less good because, while the turning points are reasonably far outside

	Numerical	Eq. (15)	Eq. (23)
μ_0	.00039	.00042	invalid
μ_1	1.006	1.008	invalid
μ_2	2.041	2.068	invalid
μ_3	3.164	3.406	invalid
μ_4	4.454	invalid	4.263
μ_5	5.973	invalid	5.821
μ_6	7.753	invalid	7.633
μ_7	9.804	invalid	9.708
μ_8	12.129	invalid	12.053

the basin, the eigenvalue is not yet very large compared to unity. The approximations are least good when the turning point is near the wall.

b. Basin [−5,1.7]

The first eight eigenfunctions are shown in Figure 3. In this case, only the lowest eigenfunction has both turning points inside the basin. Eigenfunctions 1 through 7 have the northern turning point outside the basin and the southern one inside the basin. Eigenfunction 8 (not shown) has its southern turning point right at the boundary, and eigenfunctions 9 and above have both their turning points outside the basin.

	Numerical	Eq. (20a)	Eq. (20b)	Eq. (15)	Eq. (23)
μ_0	.046	invalid		.053	invalid
μ_1	1.220	1.252	1.252	1.308	invalid
μ_2	2.532	2.542	2.542	invalid	invalid
μ_3	3.943	3.947	3.947	invalid	invalid
μ_4	5.424	5.526	5.426	invalid	invalid
μ_5	6.957	6.956	6.963	invalid	invalid
μ_6	8.541	8.525	8.645	invalid	invalid
μ_7	10.209	10.124	invalid	invalid	invalid
μ_8	12.025	11.749	invalid	invalid	11.343
μ_9	14.047	invalid	invalid	invalid	13.487

We see that in all cases the eigenvalues are reasonably approximated (to no worse than a few percent) by the expression (20), (15) or (23) in the appropriate regions of validity. The one exception is the eigenvalue whose eigenfunction has a turning point at the wall and this one is approximated to 10%.

c. Basin [−1.7,1.7]

Only the lowest eigenfunction in this small basin case has both turning points inside the basin, all others having both turning points outside the basin. The lowest

eigenfunction looks gaussian, all higher ones are indistinguishable from sines and cosines.

	Numerical	Eq. (15)	Eq. (23)
μ_0	.103	.107	invalid
μ_1	1.603	invalid	1.655
μ_2	3.793	invalid	3.808
μ_3	6.797	invalid	6.803
μ_4	10.645	invalid	10.648
μ_5	15.344	invalid	15.346
μ_6	20.895	invalid	20.896
μ_7	27.299	invalid	27.300
μ_8	34.557	invalid	34.558

The approximations for the lowest eigenvalue given by (15) is quite good, while the approximation (23), valid when both turning points are outside the basin, is essentially exact for the higher eigenvalues.

We can summarize the solutions to the v equation by noting simply that those low order modes whose turning points both lie within the basin resemble the unbounded solutions in the sense that the eigenvalues are exponentially close to integers and the eigenfunctions are very close to the unbounded solutions (Hermite functions) except that they are brought to zero within a local Rossby radius of deformation of the boundaries. Those high order modes whose turning points both lie outside the basin are oscillatory in structure, being quantized by the north and south walls, and to lowest order (n^2) resemble modes in a non-rotating system, the effects of β entering only to order 1.

While the low order v modes resemble their unbounded counterparts, the enforced vanishing at the boundaries leads to interesting behavior of the associated zonal velocity and height fields.

Corresponding to each eigenfunction

$$v_n = U(-\mu_n - 1/2, \sqrt{2}\, y) + b_n\, V(-\mu_n - 1/2, \sqrt{2}\, y)$$

are u and h fields given by

$$u_n = \frac{i}{\omega_n^2 - k^2}\,[\omega_n\, y\, v_n - k\, v_n']$$

$$h_n = \frac{i}{\omega_n^2 - k^2}\,[k\, y\, v_n - \omega\, v_n'] \tag{27}$$

where ω_n satisfies the dispersion relation (5).

Because the derivative of a series asymptotic to $v_n(y)$ need not be asymptotic to $\frac{dv_n}{dy}$, it proves convenient to re-express (27) in terms of U and V only. This can

be done using

$$\frac{d}{dy}\, U(-\mu -1/2, \sqrt{2}\, y) = -y\, U(-\mu -1/2, \sqrt{2}\, y) + \sqrt{2}\, \mu\, U(-\mu +1/2, \sqrt{2}\, y) \tag{28}$$

and

$$\frac{d}{dy}\, V(-\mu -1/2, \sqrt{2}\, y) = -y\, V(-\mu -1/2, \sqrt{2}\, y) + \sqrt{2}\; V(-\mu +1/2, \sqrt{2}\, y)$$

(Abramowitz and Stegun, 1965).

This yields

$$u_n(y) = i(\omega_n{}^2 - k^2)^{-1}\,[(\omega_n + k)y\, v_n(y) - \sqrt{2}\, k\, \mu_n$$

$$\cdot\, U(-\mu_n +1/2, \sqrt{2}\, y) - \sqrt{2}\, k\, b_n\, V(-\mu_n +1/2, \sqrt{2}\, y)] \tag{29a}$$

$$h_n(y) = i(\omega_n{}^2 - k^2)^{-1}\,[(\omega_n + k)y\, v_n(y) - \sqrt{2}\, \omega_n\, \mu_n$$

$$\cdot\, U(-\mu_n +1/2, \sqrt{2}\, y) - \sqrt{2}\, \omega_n\, b_n\, V(-\mu_n +1/2, \sqrt{2}\, y)] \tag{29b}$$

where ω_n and k must satisfy the dispersion relation (5).

We can illustrate the use of (29) by examining the behavior of the u and h fields corresponding to the lowest eigenvalue $\mu_0 << 1$. Consider, for convenience, a symmetric basin extending from $Y_S = -L$ to $Y_N = L$ where $L \geqslant 1$. Then

$$\mu_0 \cong 2\pi^{-1/2}\, L \exp\,[-L^2] \qquad \text{(using Eq. (15))}$$

and

$$b_0 \cong -\,(1/2)\pi\, \mu_0 \qquad \text{(using Eq. (13))}$$

and

$$\omega_0{}^2 - k^2 - \frac{k}{\omega_0} = 1 + 2\mu_0 \qquad \text{(see Fig. 1).}$$

Consider the region near ω, $k \approx 0$, where $\omega_0 \approx -k(2\mu_0 + 1)^{-1}$, so that we are on the "Rossby-Kelvin" part of the dispersion curve (the reason for this nomenclature will soon be apparent). The μ_0 and h_0 fields can thus be written

$$u_0 = \frac{i}{2\omega}\left[\; y\, v_0\,(y) - (1/\sqrt{2})U(-\mu_0 +1/2, \sqrt{2}\, y) + \frac{\pi}{2\sqrt{2}}\, V(-\mu_0 +1/2, \sqrt{2}\, y)\right] \tag{30a}$$

$$h_0 = \frac{i}{2\omega}\left[\; y\, v_0\,(y) + (1/\sqrt{2})U(-\mu_0 +1/2, \sqrt{2}\, y) - \frac{\pi}{2\sqrt{2}}\, V(-\mu_0 +1/2, \sqrt{2}\, y)\right]. \tag{30b}$$

As y gets large compared to one, the V term dominates and

$$\left.\begin{aligned} u_0 &\to \frac{i}{4\omega}\,\sqrt{\pi}\exp\,[y^2/2] \\ h_0 &\to -\frac{i}{4\omega}\,\sqrt{\pi}\exp\,[y^2/2] \end{aligned}\right\} \; y >> 1\,. \tag{31a}$$

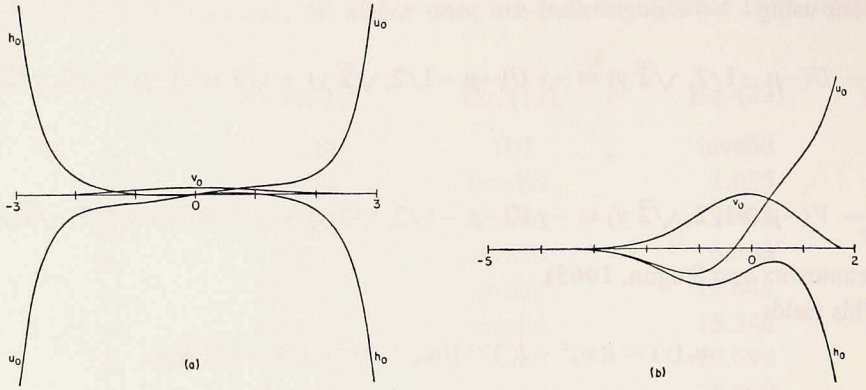

Figure 4. u, v, and h fields for the $n = 0$ Rossby-Kelvin wave. (a) In a basin $[-3,3]$, $\omega = +.5$, $k = -.501$; (b) In a basin $[-5,1.7]$, $\omega = .5$, $k = -.603$.

For y large and negative, use of (8) with $\mu_0 \approx 0$ gives

$$\left.\begin{aligned} u_0 &\to -\frac{i}{4\omega}\sqrt{\pi}\exp[y^2/2] \\ h_0 &\to \frac{i}{4\omega}\sqrt{\pi}\exp[y^2/2] \end{aligned}\right\} \; y << -1\,. \tag{31b}$$

We see that the u and h field corresponding to the lowest eigenfunction correspond to a westward propagating anti-symmetric Kelvin wave on the northern and southern wall. Figure 4a shows the u_0 and h_0 field that belongs to the lowest eigenfunction in a $[-3,3]$ basin. The amplitude of u_0 and h_0 is $0(1/\omega)$ with respect to v_0 and so is increasingly dominant at low frequency.

Using the same sort of reasoning, we can easily show that even when the frequency and wave number are not small, those parts of the $n = 0$ dispersion curve, both Rossby-Kelvin and inertia-Kelvin, that lie near $\omega + k = 0$ have their u and h fields decay exponentially away from the walls and are thus "Kelvin-like."

As we go to higher mode numbers n, b_n in (29) stays exponentially small while μ_n increases at least as n (and ultimately as n^2) so that while neither u nor h goes to zero on the boundaries, the V term no longer dominates and the behavior is not Kelvin-like near the boundaries. (Fig. 5 shows the $n = 1$ long Rossby mode in a symmetric basin.)

The two solutions left out of our catalog are those with $v \equiv 0$ and these correspond to:

(a) An eastward propagating symmetric equatorial Kelvin wave

$$u_K^- = h_K^- \sim \exp[-y^2/2], \qquad \omega = k$$

with maximum amplitude on the equator.

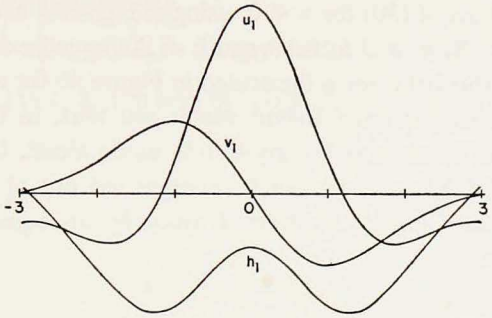

Figure 5. u, v, and h fields for the $n = 1$ Rossby mode, in a basin $[-3,3]$ $\omega = +.2$, $k = -.690$.

Because the basin is bounded, another solution exists, namely,

(b) A westward propagating symmetric "anti-"Kelvin wave

$$u_K^+ = h_K^+ \sim \exp[y^2/2], \qquad \omega = -k \tag{32}$$

with maximum amplitude at the northern and/or southern boundary.

As Moore (1968) has pointed out, the dimensional form of (32) near the northern boundary, say, can be written

$$\exp\left[\frac{1}{2}(Y_N - \eta)^2 \frac{\beta}{c}\right] = \exp\left[\frac{\beta Y_N^2}{2c}\right] \exp[-\eta/L_R] \exp\left[\frac{\eta^2\beta}{2c}\right] \tag{33}$$

where η is the distance from the northern wall and $L_R = \dfrac{c}{\beta Y_N}$ is the Rossby radius of deformation characteristic to the northern wall. Since $\dfrac{\eta^2\beta}{c} << 1$, (33) shows that the function $\exp[y^2/2]$ does indeed behave, approximately, like our usual concept of a coastal Kelvin wave, decaying exponentially away from the boundary with scale L_R.

Sums and differences of the (anti-symmetric) Rossby-Kelvin wave (Eq. (31)) and the (symmetric) anti-Kelvin wave (Eq. (32)) can be taken to produce isolated coastal Kelvin waves on either the northern or the southern boundaries in this symmetric case.

The situation is slightly different in the asymmetric case. If, say, the southern wall is much further from the equator than the northern wall, i.e., $|Y_S| >> Y_N > 1$, then the relation between b_0 and μ_0 changes to $b_0 = -\pi\mu_0$. The northern wall behavior in (30) is still dominated by the V term yielding

$$\left.\begin{aligned} u_0 &\to \frac{i}{2\omega}\sqrt{\pi}\exp[y^2/2] \\ h_0 &\to -\frac{i}{2\omega}\sqrt{\pi}\exp[y^2/2] \end{aligned}\right\} \text{ as } y \to Y_N .$$

Now, however, analysis of (30) for $y < 0$, using (8), gives a cancellation in which V no longer enters and the u_0 and h_0 fields south of the equator decay exponentially to the southern wall. (This behavior is illustrated in Figure 4b for a [−5,1.7] basin.)

Isolated northern wall-trapped Kelvin waves can thus, in this asymmetric case, be constructed out of the $n = 0$ Rossby-Kelvin mode alone. Isolated Kelvin waves trapped to the southern boundary can be constructed out of an anti-Kelvin wave (32), with the northern branch subtracted away by an equal amount of $n = 0$ Rossby-Kelvin mode.

3. Review and notation

a. Free modes

In the last section we have considered the eigenfunctions of the v equation (3) subject to zero boundary conditions on the north and south boundaries. If we define the normalized version of these eigenfunctions as

$$\psi_n(y) = v_n(y) \left[\int_{Y_S}^{Y_N} v_n^2(y)\, dy \right]^{-1/2}$$

then the normalized vector of the Fourier components of the free solutions to (1) subject to the boundary conditions (2a) (but not (2b)) can be written

$$[u,v,h] = \Phi_{n,j}(k,y)\, e^{i(kx-\omega_{n,j}(k)t)} \tag{34}$$

where n labels the mode number 0, 1 . . . . ∞ and j represents one of the 3 solutions to the dispersion relation (5).

Let us introduce the auxiliary vectors, as in I and II;

$$\mathbf{W}_n(y) = (y\,\psi_n(y),\, 0,\, -\psi_n'(y)) \tag{35a}$$

$$\mathbf{V}_n(y) = (0,\, \psi_n(y),\, 0) \tag{35b}$$

and

$$\mathbf{M}_n(y) = (-\psi_n'(y),\, 0,\, y\psi_n(y)) \tag{35c}$$

and the vector product

$$[\mathbf{A}(y),\mathbf{B}(y)] = \int_{Y_S}^{Y_N} [A_1^*\, B_1 + A_2^*\, B_2 + A_3^*\, B_3]\, dy$$

in terms of which it is easy to derive the following properties of the auxiliary functions directly from the defining Eq. (3):

$$\begin{aligned} [\mathbf{W}_m,\mathbf{W}_n] &= (2\mu_n + 1)\,\delta_{mn} & [\mathbf{W}_m,\mathbf{M}_n] &= \delta_{mn} \\ [\mathbf{M}_m,\mathbf{M}_n] &= (2\mu_n + 1)\,\delta_{mn} & [\mathbf{M}_m,\mathbf{V}_n] &= 0 \\ [\mathbf{V}_m,\mathbf{V}_n] &= \delta_{mn} & [\mathbf{W}_m,\mathbf{V}_n] &= 0\,. \end{aligned} \tag{36}$$

The free solutions (34) then become

$$\mathbf{\Phi}_{n,j}(k,y) = [\omega_{n,j}(k)\mathbf{W}_n + k\,\mathbf{M}_n(y) - i(\omega_{n,j}^2 - k^2)\,\mathbf{V}_n(y)]\,N_{n,j}^{-1} \tag{37}$$

for $n = 0, 1 \ldots$ and $j = 1, 2, 3$, where the normalization factor $N_{n,j}$ is given by

$$N_{n,j}^2 = (2\mu_n + 1)\,(\omega_{n,j}^2 + k^2) + 2k\,\omega_{n,j} + (\omega_{n,j}^2 - k^2)^2 .$$

These functions are complete, as shown in the Appendix, and have the orthonormality property

$$[\mathbf{\Phi}_{m,i}, \mathbf{\Phi}_{n,j}] = \delta_{nm}\,\delta_{ij} . \tag{38}$$

In addition, it proves useful to introduce a vector which has $v = 0$ and whose u and h components are proportional to the Rossby ($\omega \approx -k(2\mu_n + 1)^{-1}$) limits of (37):

$$\mathbf{R}_n = (4\mu_n\,(\mu_n + 1))^{-1}\,[(2\mu_n + 1)\,\mathbf{M}_n - \mathbf{W}_n] \tag{39}$$

which has the following properties:

$$[\mathbf{R}_m,\mathbf{R}_n] = (2\mu_n + 1)\,(4\mu_n\,(\mu_n + 1))^{-1}\,\delta_{mn}$$
$$[\mathbf{W}_m,\mathbf{R}_n] = 0,\ [\mathbf{M}_m,\mathbf{R}_n] = 0 . \tag{40}$$

The $v \equiv 0$ modes discussed in Section 2 are written:

$$(u,0,h) = \mathbf{\Phi}_{K,\pm 1}(y)\,\exp\,[ik(x \pm t)]$$

where

$$\mathbf{\Phi}_{K,\pm 1}(y) \equiv \mathbf{M}_K^{\pm} = 2^{-1/2}\,(\psi_K^{\pm},0,\mp\psi_K^{\pm}) \tag{41}$$

and

$$\psi_K^{\pm}(y) = a^{\pm}\,\exp\,[\pm y^2/2]$$

is normalized by $a^{\pm} = \left[\int_{Y_S}^{Y_N} \exp\,[\pm y^2/dy\right]^{-1/2}$. The $\mathbf{M}_K^{\pm}$ are normalized and mutually orthogonal. The "minus" solution is the equatorial Kelvin wave while the "plus" solution is the symmetric anti-Kelvin wave with maximum amplitude along the northern and southern boundaries.

It is easily verified that $[\mathbf{M}_K^{\pm},\mathbf{W}_n] = [\mathbf{M}_K^{\pm},\mathbf{M}_n] = 0$ so that $[\mathbf{M}_K^{\pm},\mathbf{R}_n] = 0$.

If either Y_S or Y_N recedes to infinity the anti-Kelvin wave is no longer a solution. If both Y_S and Y_N recede to infinity then the anti-Kelvin mode $\mathbf{\Phi}_{K,+1}$, the Rossby-Kelvin mode $\mathbf{\Phi}_{0,3}$, and the gravity Kelvin mode $\mathbf{\Phi}_{0,1}$ are no longer solutions. The short wave part of $\mathbf{\Phi}_{0,3}$ and $\mathbf{\Phi}_{0,2}$ then merge to produce the "mixed" mode (cf. Matsuno, 1966).

b. The x-independent forced response

The forced response to a vector of x-independent forcings $\mathbf{F} = (F,G,Q)$ switched on at $t = 0$ is, by the methods of I:

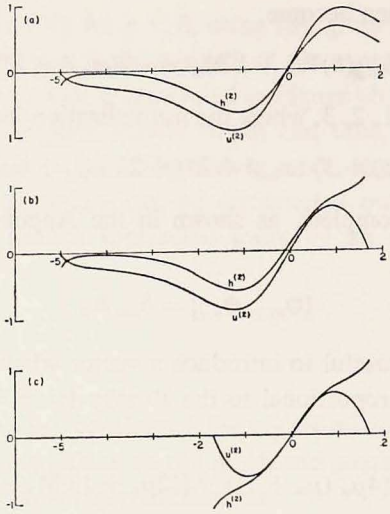

Figure 6. Zonally unbounded response to a meridional wind $G = 1$. (a) Basin $[-5,5]$ (only the part between -5 and 2 is shown—the remainder is known by symmetry); (b) Basin $[-5,1.7]$; (c) Basin $[-1.7,1.7]$.

$$\mathbf{u} = (u^{(1)}(y)t, v^{(1)}(y), h^{(1)}(y)t) + (u^{(2)}(y), 0, h^{(2)}(y)) + \mathbf{u}_I(y,t) \tag{42}$$

where

$$(u^{(1)},v^{(1)},h^{(1)}) = d_K{}^{-}\,\mathbf{M}_K{}^{-}(y) + d_K{}^{+}\,\mathbf{M}_K{}^{+} + \sum_{n=0}^{\infty} r_n\,\mathbf{R}_n - \sum_{n=0}^{\infty} (2\mu_n + 1)^{-1}\,d_n\mathbf{V}_n(y) \tag{43}$$

$$(u^{(2)},0,h^{(2)}) = \sum_{n=0}^{\infty} (2\mu_n + 1)^{-1}\,g_n\,\mathbf{W}_n(y) \tag{44}$$

and

$$\mathbf{u}_I = \sum_{n=0}^{\infty} m^{-2}\left[\mathbf{W}_n(y) + \mathbf{V}_n(y)\frac{d}{dt}\right][m^{-1}\,d_n \sin mt + g_n \cos mt] \tag{45}$$

where $m = (2\mu_n + 1)^{1/2}$.

The response $(u^{(1)}\,t, v^{(1)}, h^{(1)}t)$ is due to zonal wind and mass forcings with

$$d_K{}^{\pm} = 2^{-1/2}\,(F + Q)_K{}^{\pm}$$

$$d_n = (yF + d\,Q/dy)_n$$

$$r_n = (dF/dy + yQ)_n - (2\mu_n + 1)^{-1}\,d_n$$

where the notation $(A)_n \equiv \int_{Y_S}^{Y_N} A\psi_n\,dy$.

The response $(u^{(2)}, 0, h^{(2)})$ is due to meridional wind forcings, where $g_n = (G)_n$.

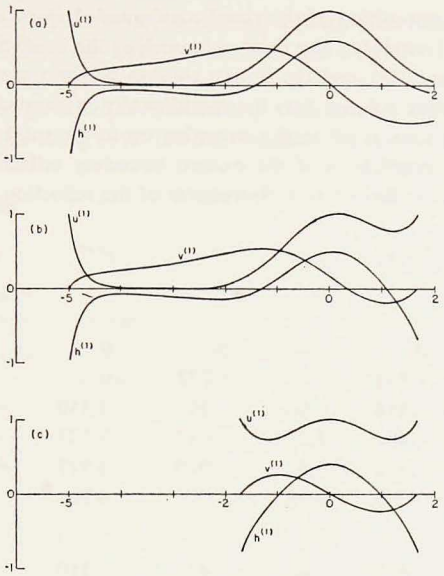

Figure 7. Same as Figure 6 but for zonal wind $F = 1$.

The response $\mathbf{u}_I$ is the initial intertial gravity response needed to set up the x-independent fields (see I and II for a thorough discussion).

By applying the operator $L \equiv \left(\frac{d^2}{dy^2} - y^2\right)$ with zero boundary conditions at Y_S and Y_N, it is easy to see from (44) and (3) that

$$L(-u^{(2)}/y) = L\left(\int_{Y_S}^{y} h^{(2)}\, dy\right) = G \tag{46}$$

Figure 6 shows the results of solving (46) numerically in the three basins of interest for $G = 1$.

Similarly, applying L to the $v^{(1)}$ part of (43) gives

$$L(v^{(1)}) = yF \tag{47a}$$

and in terms of this solution

$$h^{(1)} = -v_y{}^{(1)} \tag{47b}$$

$$u^{(1)} = F + yv^{(1)}\,. \tag{47c}$$

Figure 7 shows the results of solving (47a, b, c) in the three basins of interest for $F = 1$.

c. Examples

The modal decompositions of $\mathbf{u}^{(1)}$ and $\mathbf{u}^{(2)}$ are given, for five different north-south basins, in Tables 1 and 2 for the specific cases $F = 1$ and $G = 1$, respectively.

Table 1. The modal decomposition of the zonally unbounded response $\mathbf{u}^{(1)}$ to $F = 1$ and its reflection at the eastern boundary. The third column lists the coefficients entering the secularly growing part of (42) and (43), and the fourth column lists the coefficients of the steady part of this response. The fifth column lists the meridionally integrated zonal mass flux for each mode entering $\mathbf{u}^{(1)}$, the sum of all modes summing up to the total in the eighth column. The sixth column gives the coefficients of the eastern boundary reflection of $\mathbf{u}^{(1)}$ in Eq. (54) and the seventh the zonal mass flux of each component of the reflection.

Basin	Mode	$d_K^{\pm}, r_n$	d_n	$U^{(1)}$	c^{refl}	U^{refl}	$\int_{Y_S}^{Y_N} u^{(1)}\,dy$
$[-\infty,\infty]$							2.122
	$K(+)$	0	—	0	0	0	
	$K(-)$	1.331	—	1.772	0	0	
	1	− .888	2.663	.295	3.550	−1.181	
	3	− .466	3.261	.032	3.727	− .253	
	5	− .331	3.646	.010	3.977	− .122	
	7	− .263	3.938	.005	4.200	− .074	
[−5,5]							2.504
	$K(+)$	.655	—	.429	−1.310	− .858	
	$K(-)$	1.331	—	1.773	0	0	
	1	− .888	2.663	.296	3.550	−1.182	
	3	− .466	3.259	.032	3.724	− .254	
	5	− .329	3.623	.010	3.951	− .122	
	7	− .251	3.774	.004	4.035	− .073	
[−3,3]							2.874
	$K(+)$	.931	—	.867	−1.862	−1.733	
	$K(-)$	1.328	—	1.764	0	0	
	1	− .831	2.502	.257	3.333	−1.033	
	3	− .315	2.311	.014	2.623	− .116	
	5	− .121	1.566	.001	1.687	− .015	
	7	− .051	1.502	$\sim 10^{-4}$	1.104	− .022	
[−1.7,1.7]							2.883
	$K(+)$	1.175	—	1.381	−2.350	−2.761	
	$K(-)$	1.223	—	1.496	0	0	
	1	− .326	1.372	.027	1.698	− .139	
	3	− .052	.756	$\sim 10^{-4}$	.808	− .003	
	5	− .014	.487	0	.502	0	
	7	− .006	.358	0	.364	0	
[−5,1.7]							2.660
	$K(+)$	.463	—	.251	− .927	− .431	
	$K(-)$	1.277	—	1.631	0	0	
	0	− .353	.384	.702	.737	−1.468	
	1	− .629	2.163	.126	2.792	− .558	
	2	− .225	1.362	.009	1.588	− .061	
	3	− .275	2.442	.009	2.718	− .086	
	4	− .166	1.964	.002	2.130	− .030	

Table 2. The modal decomposition of the zonally unbounded response $\mathbf{u}^{(2)}$ to $G = 1$ and its reflection at the eastern boundary. The third column lists the coefficients $g_n = (1)_n$ in Eq. (44), the fifth column lists the meridionally integrated zonal mass flux for each mode. The fourth column lists the coefficients of the eastern boundary reflection in Eq. (55), while the sixth gives the reflected mass corresponding to it. The last column gives the constant h_0 in Eq. (55).

Basin	Mode	g_n	c	$U_n^{(2)}$	U^{refl}	$\int_{Y_S}^{Y_N} u^{(2)}\,dy$	h_0
$[\infty,\infty]$						0	0
	0	1.883	0	0	0		
	2	1.331	6.390	0	0		
	4	1.153	10.249	0	0		
	6	1.053	13.602	0	0		
$[-5,5]$						0	0
	0	1.883	5.91×10^{-10}	0	0		
	2	1.331	6.390	0	0		
	4	1.153	10.249	0	0		
	6	1.041	13.457	0	0		
$[-3,3]$						0	0
	0	1.871	.0975	0	0		
	2	1.186	6.610	0	0		
	4	.728	9.353	0	0		
	6	.440	10.905	0	0		
$[-1.7,1.7]$						0	0
	0	1.623	1.750	0	0		
	2	.635	9.373	0	0		
	4	.353	14.770	0	0		
	6	.244	20.212	0	0		
$[-5,1.7]$						−1.596	.0986
	$K(+)$	—	2.167	—	1.004		
	0	1.762	.241	−.620	−.480		
	1	.348	1.822	−.217	.364		
	2	1.053	4.801	−.237	.183		
	3	.466	5.352	−.128	.168		
	4	.836	7.898	−.139	.111		
	5	.468	8.382	−.082	.099		
	6	.684	9.696	−.080	.063		
	7	.352	8.660	−.037	.043		

Table 1 (continued).

5	− .175	2.611	.002	2.786	− .033
6	− .117	2.109	.001	2.225	− .014
7	− .106	2.263	.001	2.369	− .012
8	− .060	1.511	$\sim10^{-4}$	1.562	− .003

For the $G = 1$ case, $g_n = (1)_n$, so that in basins symmetric with respect to the equator, only even (symmetric) modes enter, while in the [−5,1.7] basin, all modes enter. Since they are orthogonal to the forcing (0,G,0), note that neither the Kelvin nor the anti-Kelvin waves can enter the sum for $\mathbf{u}^{(2)}$. The meridionally integrated zonal mass flux is defined for each mode $\mathbf{u}_n{}^{(2)}$ of (44) as

$$U_n{}^{(2)} \equiv \int_{Y_S}^{Y_N} u_n{}^{(2)}\, dy = (1)_n(y)_n(2\mu_n + 1)^{-1}$$

where (44) and the definitions (35) have been used. Only in the asymmetric basin [−5,1.7] does $U^{(2)}$ have any meridionally integrated zonal mass flux—in the symmetric basins $(1)_n(y)_n = 0$ for each mode by symmetry considerations; Figure 6 makes this clear.

For the $F = 1$ case, the coefficients of the part of (43) that varies as t are $d_K{}^- = 2^{-1/2}(1)_K{}^-$, $d_K{}^+ = 2^{-1/2}(1)_K{}^+$, and $r_n = -(2\mu_n + 1)^{-1}\,(y)_n$ and are listed in the third column of Table 1. The meridionally integrated zonal mass flux corresponding to these modes are $U_K{}^- = 2^{-1}\,[(1)_K{}^-]^2$, $U_K{}^+ = 2^{-1}\,[(1)_K{}^+]^2$, and $U_n = [(y)_n]^2\,[4\mu_n(\mu_n + 1)\,(2\mu_n + 1)]^{-1}$ and these fluxes are shown in the fifth column.[3]

It is of special interest to note that for those basins symmetric about the equator, the anti-Kelvin part of $\mathbf{u}^{(1)}$ carries more mass flux as the basin gets smaller. $\mathbf{u}^{(1)}$ in the infinite basin has no anti-Kelvin part (by the requirement of boundedness). As we go to the [−5,5] basin, the lowest few modes are essentially unchanged from the unbounded case because their turning points are still well within the basin. Essentially the only difference between the unbounded case and the [−5,5] case is the anti-Kelvin contribution, as can be seen graphically in Figure 7a. As the basin gets smaller, the anti-Kelvin mode increases in importance until we get to the [−1.7,1.7] basin where we see that essentially all the zonal mass flux in $\mathbf{u}^{(1)}$ can be accounted for solely by the Kelvin and anti-Kelvin modes.

4. The responses due to meridional boundaries

Our method, as in Papers I and II, consists of calculating the zonally unbounded response and then finding the response at the meridional boundaries $x = 0$ and X_B needed to bring the zonal velocity to zero. These boundary responses eventually reach the other boundary where they generate additional boundary responses, again those needed to bring the zonal velocity to zero. The detailed sequences of events leading to spin-up will be described in the next section. This section will show how to calculate all the needed boundary responses for use in the following section.

We should, at the outset, make clear the relation between the method used in the

3. Note that the total mass flux in the zonally unbounded solution listed in the eighth column of Table 1 and the seventh of Table 2 is reached by numerically integrating $u^{(1)}$ and $u^{(2)}$, respectively. The failure of the modal sums to add to the total in the basin cases is a measure of the total incurred error and nowhere exceeds half a percent.

meridionally unbounded case in II (Moore's algorithm; Moore and Philander, 1977) and the method used here. Moore's algorithm depends on the detailed properties of the Hermite functions whereby the u_n and h_n field corresponding to meridional velocity v_n have components only involving Hermite functions $n+1$ and $n-1$. Thus at each boundary u_n is cancelled only by contributions from u_{n+1} and u_{n-1} and Moore's algorithm results. In the meridionally bounded case, however, the eigenvalues do not differ by integers so that while u_n can be expressed as parabolic cylinder functions of order $\mu_n \pm 1$, these same cylinder functions are not also parts of $u_{n\pm1}$: Moore's algorithm fails. The method we used instead is one of projections. In the meridionally unbounded case, we have already demonstrated a unique correspondence between projection coefficients and the coefficients of Moore's algorithm (Eq. (17) of II). In the meridionally bounded case only the projection method survives.

a. Western boundary response

The zonally unbounded solution (Eq. (42)) has planetary wave parts varying only as t^s ($s = 0$ or 1). The western boundary response must consist of a Kelvin wave plus a sum of terms composed of short wavelength Rossby waves: these are the only planetary modes with group velocity to the east. This response may be written, as in II:

$$\mathbf{u}^W(x,y,t) = b_K H(t-x)(t-x)^s \mathbf{M}_K{}^-(y) + \mathbf{u}^B(x,y,t) \tag{48}$$

where, to the lowest order in t/x, $\mathbf{u}^B$ is nondivergent with its *meridional* velocity component in geostrophic balance with the height field:

$$\mathbf{u}^B \equiv (u^B,v^B,h^B) = \left[-\frac{\partial}{\partial y}, \frac{\partial}{\partial x}, y \right] \left\{ \left(\frac{t}{x}\right)^{s/2} J_s(2\sqrt{xt})\,\chi(y) \right\} \tag{49}$$

with

$$\chi(y) = \Sigma b_n \psi_n(y)\,.$$

Because $\chi = 0$ at Y_S and Y_N it is clear that $\int_{Y_S}^{Y_N} u^B(x,y,t)\,dy = 0$. Thus, since $u^W + u(y)t^s = 0$ at $x = 0$, we can integrate to yield

$$b_K = -2^{1/2}[(1)_K{}^-]^{-1} \int_{Y_S}^{Y_N} u(y)\,dy \tag{50}$$

where

$$(1)_K{}^- \equiv \int_{Y_S}^{Y_N} \psi_K{}^-\,dy$$

is simply the projection of 1 on the Kelvin mode, and is known for each basin.

Thus, as in II, the Kelvin amplitude is determined by noting that all the incident zonal mass flux onto the western boundary is returned by the Kelvin wave. An ob-

vious corollary that will prove useful in what follows is that no Kelvin wave is excited off the western boundary when the incident integrated zonal mass flux vanishes.

With b_K known,

$$\chi(y) = \int_{Y_s}^{y} [u(y) + 2^{-1/2}\, b_K\, \psi_K{}^-(y)]\, dy \tag{51}$$

and the b_n's can be obtained by projection from the now known function $\chi(y)$.

Any Rossby, Rossby-Kelvin, or anti-Kelvin modes emitted as part of the eastern boundary response (described below) produce a western boundary response that can be calculated exactly as described above. In particular, all the meridionally integrated zonal mass flux is returned by the Kelvin wave.

b. Eastern boundary response

We have to calculate the eastern boundary response needed to bring the unbounded zonal velocity to zero and to reflect any Kelvin waves emitted by the eastern boundary.

As in II, we can use (1b) and (2a) to conclude that, asymptotically, the effect of the incident Kelvin mode and its reflections in the anti-Kelvin and Rossby modes is simply to raise the height uniformly (in y) at the eastern boundary by an amount A:

$$\mathbf{M}_K{}^- + a_K{}^+\, \mathbf{M}_K{}^+ + \sum_{n=0}^{\infty} a_n\, \mathbf{R}_n = (0, 0, A)\,. \tag{52}$$

Taking projections successively with $\mathbf{M}_K{}^-$, $\mathbf{M}_K{}^+$ and $\mathbf{R}_m$ yields

$$A = 2^{1/2}/(1)_K{}^- \tag{53a}$$

$$a_K{}^+ = -A\, 2^{-1/2}\, (1)_K{}^+ = -\,(1)_K{}^+/(1)_K{}^-\,, \tag{53b}$$

and

$$a_n = A(y)_n = 2^{1/2}\, (y)_n/(1)_K{}^-\,. \tag{53c}$$

We can also see from (52) and (53) that the meridionally integrated mass flux associated with the reflected anti-Kelvin wave is in the opposite direction to the meridionally integrated mass flux associated with the incident Kelvin-wave. The Rossby waves (including the $n = 0$ Rossby-Kelvin wave) must carry off the difference of the mass fluxes due to the Kelvin and anti-Kelvin waves.

The eastern boundary response needed to bring the zonally unbounded response to a zonal current in (43) and (44), of form $u(y)t^s$ to zero will have the general form

$$\mathbf{u}^E = c_K{}^+\, \zeta_K{}^s\, H(\zeta_K)\, \mathbf{M}_K{}^+ + \sum_{n=0}^{\infty} c_n\, H(\zeta_n)\, \{\zeta_n{}^s\, \mathbf{R}_n + s\, \mathbf{V}_n\} \tag{54}$$

where

$$\zeta_n = t + (2\mu_n + 1)\, (x - X_E)$$

and

$$\zeta_K = t + x - X_E \,.$$

The response to the Rossby and anti-Kelvin mode in (43), for example, is the corresponding free mode with the same structure. Thus $t\, r_n\, \mathbf{R}_n$ generates an eastern boundary response $-r_n\, \zeta_n\, H(\zeta_n)\mathbf{R}_n$ and $td_K{}^+\, \mathbf{M}_K{}^+$ generates an eastern boundary response $-d_K{}^+\, \zeta_K\, H(\zeta_K)\mathbf{M}_K{}^+$. The eastern boundary response to the Kelvin part of (42) is found in an obvious way using Eq. (53) to find the reflected coefficients.

The eastern boundary response to the unbounded response generated by a meridional wind, (44), is a bit different. The bondary condition at $x = X_E$ is that $u^{(2)} + u^E = 0$. Since $v^{(2)} = 0$ and $s = 0$ in (54) we have that $v^{(2)} + v^E = 0$ and it then follows from (2b) that $h_y = G$. A concise statement of the preceding argument is that, at $x = X_E$,

$$(u^{(2)},0,h^{(2)}) + c_K{}^+\, \mathbf{M}_K{}^+ + \sum_{n=0}^{\infty} c_n\, \mathbf{R}_n = (0,0, \int_0^y G\, dy + h_0) \tag{55}$$

where h_0 is as yet an unknown constant. This constant can be determined by noting that the Kelvin mode $\mathbf{M}_K{}^-$ is orthogonal to each term on the left-hand side of (55). Projecting $\mathbf{M}_K{}^-$ onto (55) and using the notation $I(y;G) = \int_0^y G(y')dy'$ gives

$$h_0 = -(I)_K{}^-/(1)_K{}^- \,. \tag{56a}$$

Once h_0 is known, the c's can be found by projecting $\mathbf{M}_K{}^+$ and $\mathbf{R}_n$ onto (55):

$$c_K{}^+ = -2^{-1/2}\, (I)_K{}^+ - 2^{-1/2}\, [(1)_K{}^+]\, h_0 \tag{56b}$$

and

$$c_n = (yI)_n - g_n\, (2\mu_n + 1)^{-1} + h_0\, (y)_n \,. \tag{56c}$$

It should be emphasized that the results (48), (52) and (55) are asymptotic results and cannot be expected to hold at all times. Thus, for example, if an anti-Kelvin wave should hit the western boundary and reflect as boundary trapped modes $\mathbf{u}^B$ plus a Kelvin wave according to (48), it will take time for the Kelvin wave, whose amplitude is localized about the equator, to be produced by the anti-Kelvin wave, whose amplitude is localized near the (possibly distant) northern and southern boundaries. The necessary communication cannot be accomplished at a speed faster than the fastest wave in the problem, namely, unity. It in fact does seem to take place *at* speed unity by northward and southward propagating waves; these may be thought of as wall-Kelvin waves. Similarly, when a Kelvin wave hits the eastern boundary, the height field is raised first at the equator and then, with speed unity, to the north and south of the equator until the height is uniformly raised at the eastern boundary. The asymptotics of this process is analyzed in some detail by Anderson and Rowlands (1976).

Table 3. The eastern boundary reflection of $\mathbf{M}_K^-$. The fourth column lists the coefficients appearing in Eq. (52), the fifth lists the amount of reflected meridionally integrated zonal mass flux for each mode, and the sixth lists the quantity A in Eq. (52).

Basin	Mode	Eigenvalue	a	U/U_K^-	A
$[-\infty,\infty]$					.751
	1	1	2.000	−.500	
	3	3	2.450	−.125	
	5	5	2.739	−.063	
	7	7	2.958	−.039	
[−5,5]					.751
	$K(+)$		−.492	−.242	
	1	$1+3.92\times10^{-9}$	2.000	−.500	
	3	$3+1.63\times10^{-6}$	2.448	−.125	
	5	$5+2.04\times10^{-4}$	2.721	−.062	
	7	$7+1.22\times10^{-2}$	2.843	−.036	
[−3,3]					.753
	$K(+)$		−.701	−.491	
	1	1.006	1.884	−.440	
	3	3.164	1.741	−.058	
	5	5.973	1.179	−.008	
	7	9.804	.793	−.001	
[−1.7,1.7]					.818
	$K(+)$		−.961	−.923	
	1	1.603	1.122	−.075	
	3	6.797	.618	−.002	
	5	15.344	.398	-2×10^{-4}	
	7	27.299	.293	-3×10^{-5}	
[−5,1.7]					.783
	$K(+)$		−.363	−.132	
	0	.046	.301	−.470	
	1	1.220	1.694	−.265	
	2	2.532	1.067	−.032	
	3	3.943	1.913	−.047	
	4	5.424	1.538	−.017	
	5	6.957	2.045	−.019	
	6	8.541	1.651	−.008	
	7	10.209	1.772	−.007	
	8	12.025	1.184	−.002	

c. Examples

In this subsection we will examine the eastern boundary response to an incident Kelvin wave in five basins of interest, and the boundary response to the unbounded solutions forced by $G = 1$ and $F = 1$ in these same five basins.

Table 3 lists the low order terms in Eq. (52) for the response of a Kelvin mode of

unit amplitude, $\mathbf{M}_K{}^-$, striking the eastern boundary of five basins of different north-south extent. In the unbounded basin, the Kelvin wave reflects only in the odd n modes (whose zonal velocity is symmetric) with half of the incident meridionally integrated zonal mass flux, $U_K{}^- = 2^{-1/2}\,(1)_K{}^-$, being reflected in the $n = 1$ mode, and slowly decreasing amounts in the higher modes. Since in the unbounded case

$$\frac{U_n}{U_K{}^-} = -\frac{a_n{}^2}{4n(n+1)} = -\frac{2^{1/2}}{(1)_K{}^-}\,\frac{(y)_n{}^2}{4n(n+1)},$$

we can use the summation formula given in the Appendix of II to verify that $\sum_1^\infty U_n = -U_K{}^-$. We see from Table 3 that 27% of the zonal mass flux is returned in modes $n = 9$ and higher. Again, using the summation formula in the Appendix of II, we verify that

$$\sum_N^\infty \frac{U_n}{U_K{}^-} = -\frac{a_N{}^2}{4(N+1)} = -\frac{N!}{2^{N-1}\,(N+1)}\left[\left(\frac{N-1}{2}\right)!\,\right]^{-2} \tag{57}$$

so that

$$\sum_9^\infty U_n = -.27\,U_K{}^-.$$

When we move to the [−5,5] basin, we see that 24% of the incident Kelvin wave zonal mass flux is now returned by the anti-Kelvin wave while the amount returned by the first few Rossby waves hardly changes. In fact, we can easily verify that the anti-Kelvin mode in a basin $(-L,L)$ for $L >> 1$ reflects an amount of mass flux

$$U_K{}^+ = -[U_K{}^-]\,\sqrt{2}\,L^{-1}$$

which in turn is equal to the sum of the mass fluxes that would have been returned by all the unbounded modes whose turning point lies beyond L[4]. Thus in a bounded basin $[-L,L]$, only the modes whose turning points lie within the basin, $2\mu_n + 1 < L^2$, reflect any mass flux, while the purely oscillatory modes for which $2\mu_n + 1 > L^2$ reflect none. Thus, for the narrow basin case, [−1.7,1.7], almost all the incident Kelvin mass flux is reflected by the anti-Kelvin mode.

The western boundary response to the unbounded solution $\mathbf{u}^{(1)}$ and $\mathbf{u}^{(2)}$, in response to $F = 1$ and $G = 1$, respectively, contains a Kelvin wave whose amplitude is such as to reflect all the mass flux, according to Eq. (50). The total zonal mass fluxes are listed in Tables 1 and 2; the b_K's are then gotten from (50).

The eastern boundary response to the unbounded solution $\mathbf{u}^{(1)}$ and $F = 1$ is given in Table 1, and to the unbounded solution $\mathbf{u}^{(2)}$ for $G = 1$ in Table 2.

4. The first part of this result is obtained by asymptotically expanding the integrals in $U_K{}^+/U_K{}^-$ in L while the second part is obtained by using (57) with $2N + 1 = L^2$ and using Stirling's formula to expand for large N.

5. Numerical simulations of time dependent response

In order to illustrate and make concrete the analytical results presented thus far, we will in this section present numerical results for the linear time-dependent response of three equatorial basins to the simple wind stress patterns $F = 1$ and $G = 1$. The first basin has its northern and southern boundaries relatively far from the equator at ± 5; the second is relatively narrow and extends from -1.7 to $+1.7$; the third is asymmetrical with its northern boundary at $+1.7$ and its southern boundary at -5. All three basins will be taken to be 10 units long in the zonal direction with the western boundary at $x = 0$ and the eastern boundary at $x = 10$. Since neither of the simple wind stresses we have chosen has curl, the steady state to which each basin will tend is simply the one in which the height field gradient balances the imposed wind stress. Thus in the $F = 1$ case, the height field in all three basins will be tilted from -5 to 5 with longitude; in the $G = 1$ case the height field will tilt uniformly with latitude from -5 to 5, -1.7 to 1.7, and -3.35 to 3.35 in the wide, narrow and asymmetric basins, respectively.

The numerical model used to simulate these ocean responses has been described elsewhere (Cane 1975, 1979). Because we ran three basins for each wind stress and each unit of nondimensional time required 60 computer time steps, practical considerations limited the total number of computer time steps to 3840 (64 nondimensional time units) for each of the six cases.

a. The F = 1 Case

We will begin discussion of the $F = 1$ case by reviewing the meridionally unbounded situation as discussed in II. As soon as the wind begins to blow, inertia-gravity waves are excited in such a way that by one or two units of non-dimensional time, the unbounded solution $(u^{(1)}t,\ v^{(1)},\ h^{(1)}t)$ has been fully developed. Also at $t = 0$ a full set of Rossby modes, $n = 1, 3, 5, \ldots$, begin propagating into the basin from the eastern boundary, and a Kelvin mode carrying the meridionally integrated zonal mass flux $\int_{-\infty}^{\infty} u^{(1)}t\, dy$ propagates into the basin from the western boundary. The initial solution is therefore:

$$\mathbf{u} = t\left[d_K^{-}\mathbf{M}_K^{-} + \sum_{n=1}^{\infty} r_n \mathbf{R}_n \right] + b_K(t-x)H(t-x)\mathbf{M}_K^{-} - \sum_{n=1}^{\infty}(2n+1)^{-1}d_n \mathbf{V}_n$$

$$+ \sum_{n=1}^{\infty}\Big\{(-r_n + d_K^{-} a_n)\,(t+(2n+1)\,(x-10))\,\mathbf{R}_n + (2n+1)^{-1}d_n\mathbf{V}_n$$

$$\cdot \quad H(t + (2n+1)\,(x-10))\Big\} \tag{58}$$

where the coefficient of the propagating Rossby modes is partly the direct eastern

boundary response to the Rossby part of $\mathbf{u}^{(1)}$ and partly the eastern boundary response to the Kelvin part of $\mathbf{u}^{(1)}$. If we note that $b_K = -\pi^{-1/4}(\pi^{1/2} + U_R)$, where $\pi^{1/2}$ and U_R are the total meridionally integrated zonal mass fluxes in the Kelvin and Rossby parts of $\mathbf{u}^{(1)}$ ($U_R = +.350$ in the unbounded case according to Table 1), and if we assume that enough time has gone by for *all* the Rossby modes to reach the point x, then (58) becomes, using (52):

$$\mathbf{u} = (0,0,x) + U_R \mathbf{M}_K^-(t-x) + 10 \Sigma r_n(2n+1)\mathbf{R}_n$$

$$+ d_K^- \sum_{n=1}^{\infty} a_n(t+(2n+1)(x-10))\mathbf{R}_n . \tag{59}$$

The $(0,0,x)$ part of (59) has the correct slope but not the correct level to be the final steady state. The additional terms are those due to the initial Kelvin mode. The second term in particular does not stay around longer than $t = 10$—it then hits the eastern boundary producing a new series of Rossby modes. The Rossby modes, when they hit the western boundary, produce new Kelvin modes. We see therefore that while the initial solution contains enough Rossby modes to bring the height field to its correct tilt, it also initiates motions which continue to slosh mass back and forth across the basin (see II for a more complete discussion).

The initial series of reflections for the unbounded case can be described as follows. At $t = 0$ a Kelvin mode of negative amplitude carrying negative mass flux leaves the western boundary while a Rossby mode leaves the eastern boundary. The effect of these modes can be easily seen on the height field section across the equator in Figure 8. (Since the meridionally unbounded case cannot be simulated numerically, these figures were generated by summing modes.) The initial Kelvin mode, carrying negative mass flux, lowers the height field while the initial Rossby wave, also carrying negative mass flux, raises it. The flat part of the height field at $t = 4$ is simply the secularly growing part $h^{(1)}t$—it grows as if zonally unbounded because the effects of the boundaries have not yet reached it. At $t = 7.5$ the initial Kelvin and first Rossby modes meet and no secularly growing flat part of the height field remains. At $t = 10$ the initial Kelvin mode hits the eastern boundary and reflects as a Rossby mode of positive mass flux: this mode lowers the height field to its east as it propagates westward with speed 1/3. Thus the height field at the eastern boundary decreases uniformly with time until $t = 40$ when the Kelvin mode, due to the reflection of the first Rossby mode, hits and starts increasing the height field uniformly with time. At the western boundary the height field decreases uniformly during times 0 to 30 whereupon the second Rossby mode arrives producing a Kelvin mode of negative mass flux; at $t = 40$ the height field again begins to fall at the west.

The situation in the meridionally bounded basin is very different. Figure 9 shows the reflection diagram for the $[-5,5]$ basin, keeping track of only the Kelvin, anti-Kelvin and $n = 1$ Rossby modes. The initial unbounded solution ($u^{(1)}t$, $v^{(1)}$, $h^{(1)}t$)

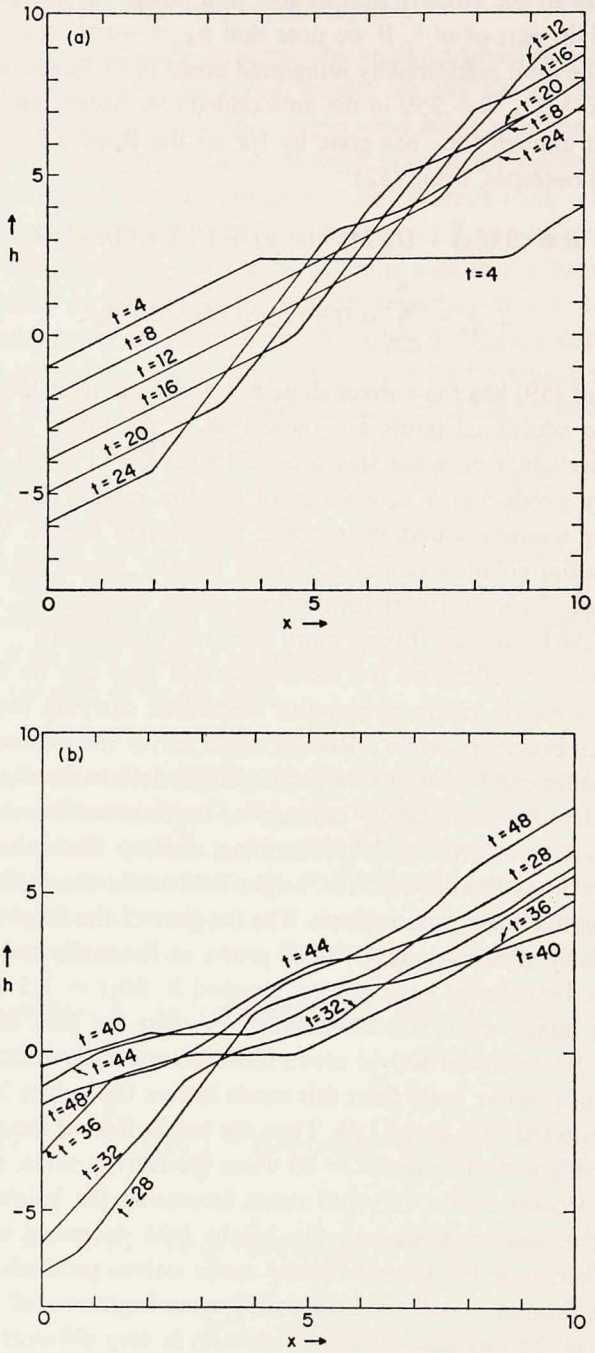

Figure 8. An equatorial section for $x = 0$ to 10 of the height field in the meridionally unbounded $F = 1$ case. (a) Times $t = 4$ to 24; (b) Times $t = 28$ to 48.

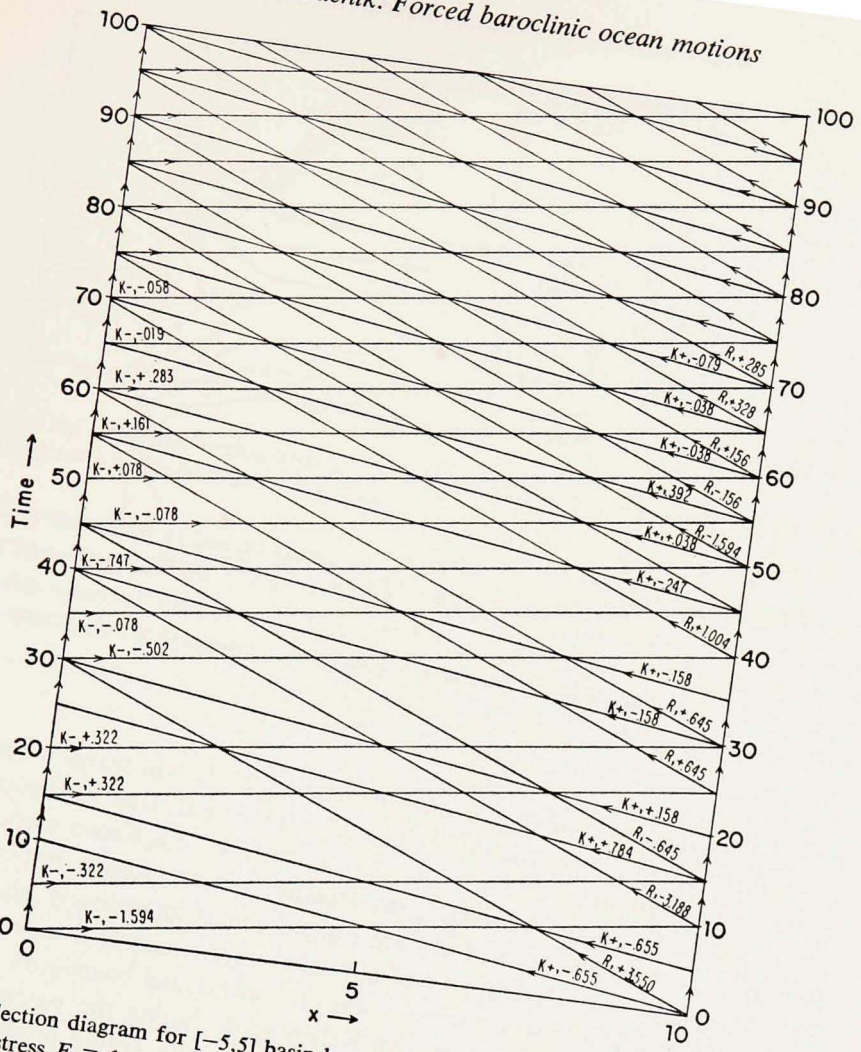

Figure 9. Reflection diagram for $[-5,5]$ basin bounded zonally at $x = 0$ and 10 subject to uniform wind stress $F = 1$. Kelvin modes ($K-$) leave the western boundary; only the $n = 1$ Rossby (R) is kept track of leaving the eastern boundary and the anti-Kelvin mode ($K+$) is also emitted at the east. The amplitudes are written next to the mode designation.

contains an anti-Kelvin mode of amplitude .655. (Note from Table 1 that the coefficients of the Kelvin and the first four Rossby modes are essentially the same as they re in the meridionally unbounded case—the major difference between the cases is e presence of the anti-Kelvin mode.) At the western boundary a Kelvin mode rects the mass flux of the Kelvin and Rossby parts of $\mathbf{u}^{(1)}$ is emitted immediately ile the Kelvin mode, which is to reflect the mass flux of the anti-Kelvin part of), cannot be emitted until the initial anti-Kelvin mode has communicated with equator. As discussed in Section 4, this communication can be thought of as

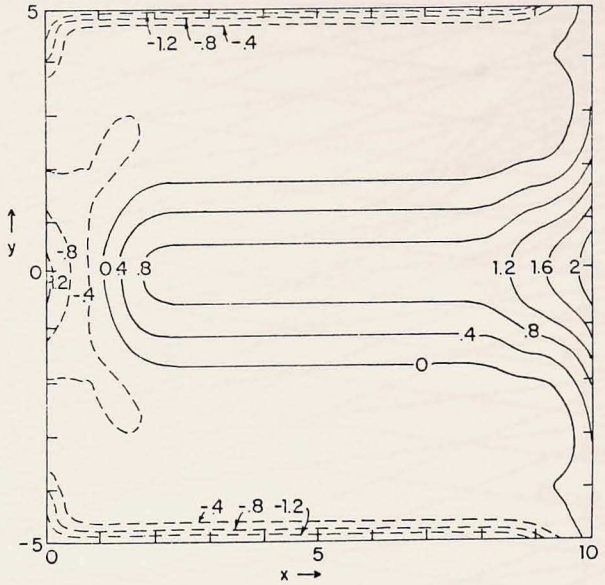

Figure 10. Contour plot of height field at $t = 2$ for $F = 1$ forcing in a $[-5,5]$ basin bounded zonally at $x = 0$ and $x = 10$.

taking place by means of equatorward travelling wall-Kelvin waves which do not reach the vicinity of the equator until $t \cong 5$—this is indicated in Figure 9 by an arrow on the western boundary leading to the emission of a Kelvin mode at $t = 5$. Similarly, at the eastern boundary, the Rossby and anti-Kelvin response to the Rossby and anti-Kelvin parts of $\mathbf{u}^{(1)}$ are emitted almost immediately while the anti-Kelvin response to the Kelvin part of $\mathbf{u}^{(1)}$ takes approximately 5 time units to develop while wall-Kelvin waves travel toward the meridional boundaries to make the connection. At later times, every anti-Kelvin mode hitting the western boundary produces a wall-Kelvin wave that travels to the equator before producing the reflected Kelvin mode and every Kelvin mode hitting the eastern boundary produces a wall-Kelvin wave that travels to the northern and southern boundaries before producing the reflected anti-Kelvin mode. The amplitudes for the various modes and reflections are given in Figure 9 until $t = 70$.

Figure 10 illustrates these initial features: it shows the height contours throughout the basin at $t = 2$. The unbounded $\mathbf{u}^{(1)}$ solution (compare to Fig. 7a) is clearly visible in the center of the basin where neither the Kelvin nor the first Rossby have yet arrived. On the western boundary, the deepening effect of the first Kelvin wave extending to $x = 2$ is seen, and near the northern and southern boundaries the anti-Kelvin part of $\mathbf{u}^{(1)}$ turning the corner as a wall-Kelvin is seen. At the eastern boundary the Rossby mode should extend 2/3 of a unit into the basin but inevitably

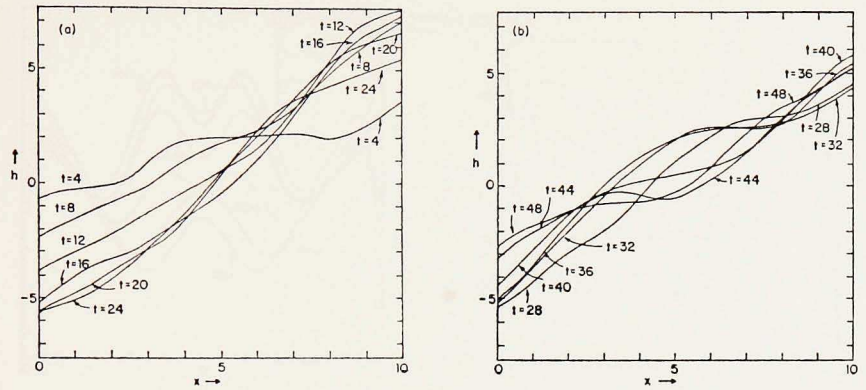

Figure 11. An equatorial section from $x = 0$ to 10 of the height field in the $[-5,5]$ $F = 1$ case. (a) Times $t = 4$ to 24; (b) Times $t = 28$ to 48.

precursors travelling as fast as speed unity produce wiggles that extend a full 2 units into the basin (see Section 3 of Paper I for a discussion of precursors and the dispersive modification of propagating Rossby fronts). The initial anti-Kelvin mode of negative amplitude (therefore positive height field) is seen propagating westward and cancelling the negative height (growing with t) anti-Kelvin mode of the unbounded solution. Finally, the wall-Kelvin (of positive height) is seen propagating toward the northern and southern boundaries. A similar contour plot 2 time units later would show these trends continuing—the unbounded solution $\mathbf{u}^{(1)}$ continuing to grow as t, the initial Kelvin mode continuing to lower the height field behind it as it propagates eastward, and the initial Rossby mode continuing to raise the height field behind it as it propagates westward, while the wall-Kelvin waves continue their journey along the eastern and western boundaries.

We can follow the progress of the system in time by examining Figure 11a, an equatorial slice of the height field from the eastern to western boundary. The deepening at the western boundary behind the initial Kelvin front proceeds faster than the comparable meridionally unbounded case in Figure 8a between times 4 and 16 because of the additional emission of the Kelvin mode of negative amplitude at $t = 5$ due to the reflection of the anti-Kelvin part of $\mathbf{u}^{(1)}$ in the basin case.[5] This more rapid deepening continues until $t = 15$ when the emission of a Kelvin mode of positive amplitude slows the deepening rate back to what it was in the meridionally unbounded case. At $t = 20$ another Kelvin mode of positive amplitude is emitted and the deepening slows even more. At the eastern boundary, the raising of the height field behind the initial Rossby mode emitted at $t = 10$ proceeds as in the meridionally unbounded case until $t = 15$ when a Kelvin mode of negative amplitude arrives and is reflected as a set of Rossby modes of negative amplitude. The lowering of the

5. The height field at $t = 4$ at the west is not as deep as in the meridionally unbounded Figure 8a because the wind stress had to be turned on gradually over the first time period for numerical reasons.

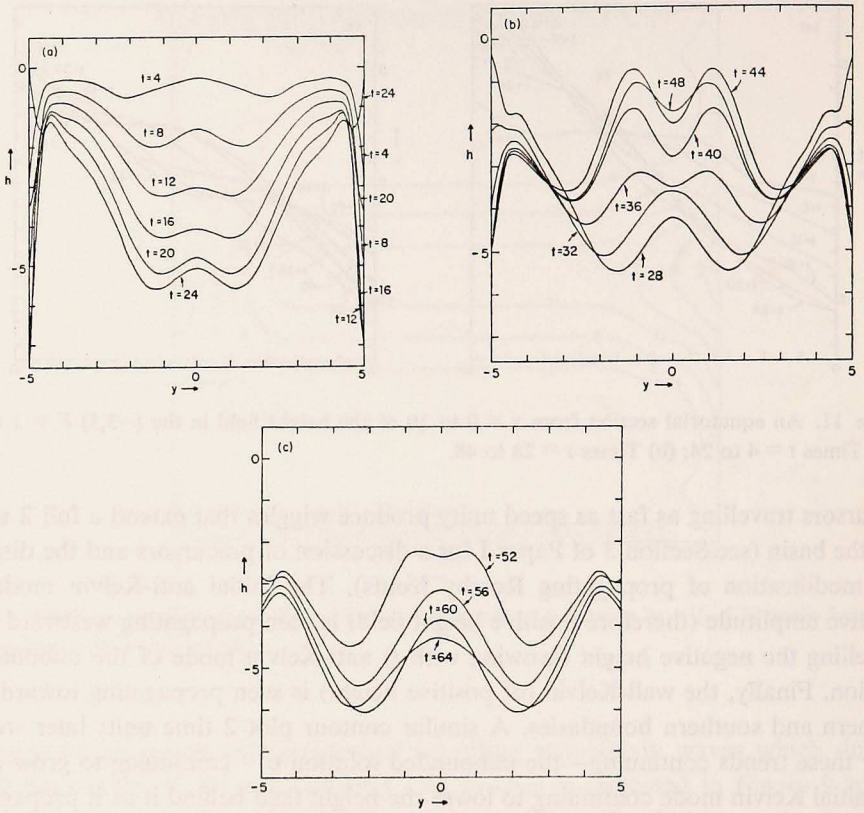

Figure 12. A meridional section of the height field at $x = 1$ from [−5,5] for the $F = 1$ case. (a) Times $t = 4$ to 24; (b) Times $t = 28$ to 48; (c) Times $t = 52$ to 64.

height field between $t = 10$ and $t = 25$ therefore proceeds faster than in the meridionally unbounded case. Note in Figure 11a that despite the fact that the fronts have been smoothed by dispersion relative to Figure 8a, it is still possible to trace the Kelvin and the larger Rossby fronts across the basin.

At $t = 30$ the first $n = 1$ Rossby mode hits the western boundary emitting a positive amplitude Kelvin mode and at $t = 40$ the second negative amplitude Rossby mode hits the boundary emitting a negative Kelvin mode. The height field at the western boundary should then begin to increase at $t = 30$ and decrease at $t = 40$. Figure 11b, however, shows that the height field increases very slowly from $t = 32$ to 40 and continues to increase from $t = 40$ to $t = 48$ (it starts decreasing rapidly only after $t = 48$). What is happening is that wall-Kelvin waves hanging around from previous reflections are contaminating the results at the equator.

We can remove this contamination and see more clearly the progress of the response by examining a meridional slice of the height field at $x = 1$ (Fig. 12). As we

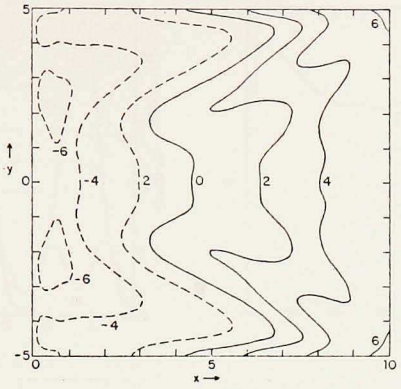

Figure 13. Same as Figure 10 but at $t = 64$.

have seen, the deepening proceeds rapidly from $t = 4$ to 20 (Fig. 12a). The slowing of the deepening at $t = 20$ and 24 due to the emission of the Kelvin modes at the western boundary at $t = 15$ and 20 is clearly seen as is the arrival of the anti-Kelvin modes at $t = 9$ and 14 which reverse the anti-Kelvin amplitude. The first Rossby hits $x = 1$ at $t = 29.7$ and by $t = 36$ (Fig. 12b) the characteristic $n = 1$ Rossby structure (compare to Fig. 5) has grown strong enough to be seen in the height field. The arrival of the strong anti-Kelvin at $t = 24$ begins to lower the anti-Kelvin amplitude as is clear in Figure 12b. The arrival of the second Rossby at $t = 39.7$ and its reflected negative amplitude Kelvin at $t = 41$ is most clear in the height field for $t = 52$ (Fig. 12c) where the large Rossby amplitude from the first (positive) Rossby mode has been effectively cancelled by the arrival of the second (negative) Rossby mode—only a remnant is left by $t = 52$. The arrival of the positive Rossby at $t = 59.7$ is slightly evident in the $t = 64$ curve.

A contour plot (Fig. 13) of the height field at $t = 64$ (the last time computed) shows that the height field is relatively well set up along the equatorial regions, less well set up away from the equator, and still less well set up away from the equator toward the west. This is understandable in terms of the large number of initial Rossby modes, $n = 1, 3, 5$, etc., that have reached longitudes close to the eastern boundary—at the other end of the basin, however, the $n = 3$ Rossby mode has not yet reached the western boundary by $t = 64$.

The gross energetics of the spin-up process are summarized by Figure 14a which shows potential and kinetic energy as a function of time. The kinetic energy is increasing rapidly with time until $t = 7.5$ when the initial Kelvin and Rossby modes meet and the initial rapid acceleration stops. The potential energy continues to increase as the initial Kelvin mode lowers the height at the west and the initial Rossby raises it at the east. It reaches a peak (i.e., the height field is maximally tilted) between $t = 16$ to 20 and then begins to decline as the emitted Kelvin modes in the

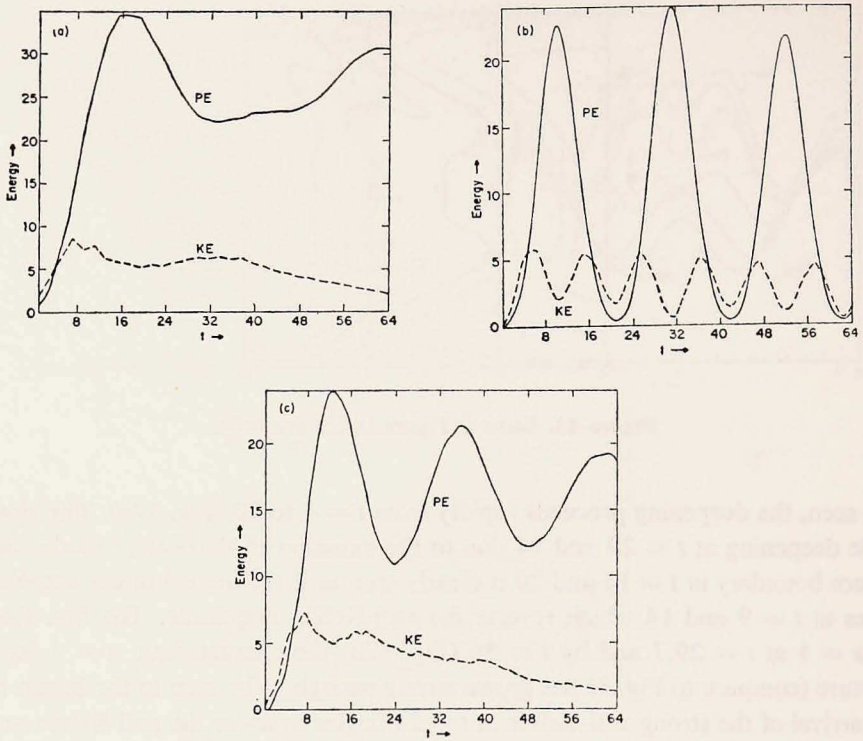

Figure 14. Energy versus time for the $F = 1$ case. (a) Basin [−5,5]; (b) Basin [−1.7,1.7]; (c) Basin [−5,1.7]. Units arbitrary.

west and the second Rossby mode in the east act to reduce the overall east-west tilt. The subsequent periodicity is approximately 40 time units—the roundtrip time of a Kelvin-Rossby mode transit.

The Rossby modes lose their importance in the [−1.7,1.7] case as can be seen from Tables 2 and 3. We may thus understand this case almost entirely in terms of the Kelvin and anti-Kelvin modes (since the northern and southern boundaries are so close to the equator there is considerable overlap between the Kelvin and anti-Kelvin modes and the delay due to the travel of the wall-Kelvin is substantially absent). The initial Kelvin mode emitted from the east at $t = 0$ has an amplitude of −2.36, carries all the mass flux of the meridionally unbounded solution (−2.88), and lowers the height field behind it as it propagates toward the east. The initial anti-Kelvin emitted from the east has amplitude −2.35, carries mass flux −2.76, and *raises* the height field as it propagates westward. Since both the Kelvin and anti-Kelvin work to increase the east-west tilt, the potential energy will increase monotonically until $t = 10$ when the Kelvin mode hits the western boundary. Since the anti-Kelvin mode carried almost all the mass flux, it reflects as a Kelvin mode of

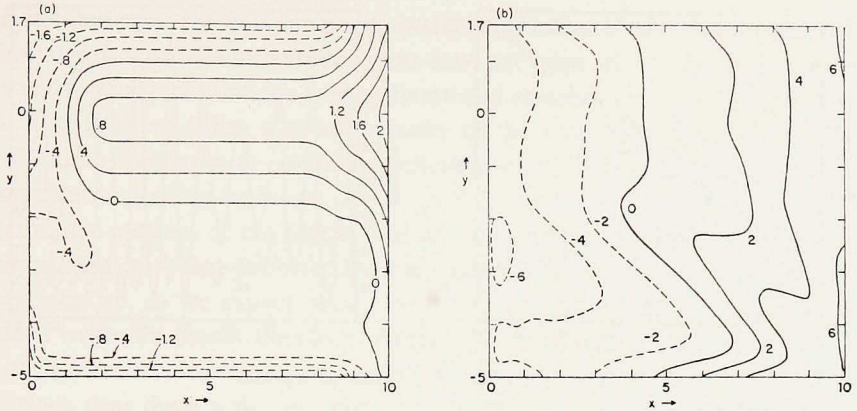

Figure 15. Same as Figure 10 but for a [−5,1.7] basin. (a) $t = 2$; (b) $t = 64$.

amplitude +2.26 which tends to raise the height field behind it. Similarly, the Kelvin mode reflects at the eastern boundary as an anti-Kelvin mode of amplitude +2.27, which now tends to lower the height field behind it. By $t = 20$ almost all the tilt induced by the initial Kelvin-anti-Kelvin pair is wiped out by the reflected anti-Kelvin-Kelvin pair: the height field becomes almost flat. The potential energy therefore has a periodicity of 20 time units and it almost reaches zero at its minimum; Figure 14b. The kinetic energy is largest when the height field is changing most rapidly and so has a periodicity half that of the potential energy.

The asymmetric basin [−5,1.7] provides an intermediate case, containing some features of both the wide basin and narrow basin case, as well as some features uniquely its own. Because of the lack of symmetry with respect to the equator, *all* modes will be excited. Tables 2 and 3 show that the $n = 0$ Rossby-Kelvin mode (Fig. 4b) is especially important in this asymmetric basin. Figure 15a shows the height field at $t = 2$. Now the amplitude on the northern wall is mostly Rossby-Kelvin while the amplitude on the southern wall is predominately anti-Kelvin. The dominant periodicity is now $t = 20$, the Rossby-Kelvin-Kelvin roundtrip transit time but, as can be seen in Figure 14c, the successive peaks are delayed because of the transit time of the wall-Kelvins needed to communicate between the Kelvin and anti-Kelvin modes. The state at the end of 64 time units, Fig. 15b, shows the height field evenly tilted in the northern part of the basin but again less well spun up in those parts of the southern region where the higher Rossby modes have yet to reach. Even in the northern regions, however, the height field continues to undergo oscillations as the Kelvin mode sloshes mass across the basin.

b. The $G = 1$ case

In the meridionally unbounded situation (discussed in Paper II), the $G = 1$ forcing excites no Kelvin or anti-Kelvin modes; only even n Rossby modes. By sym-

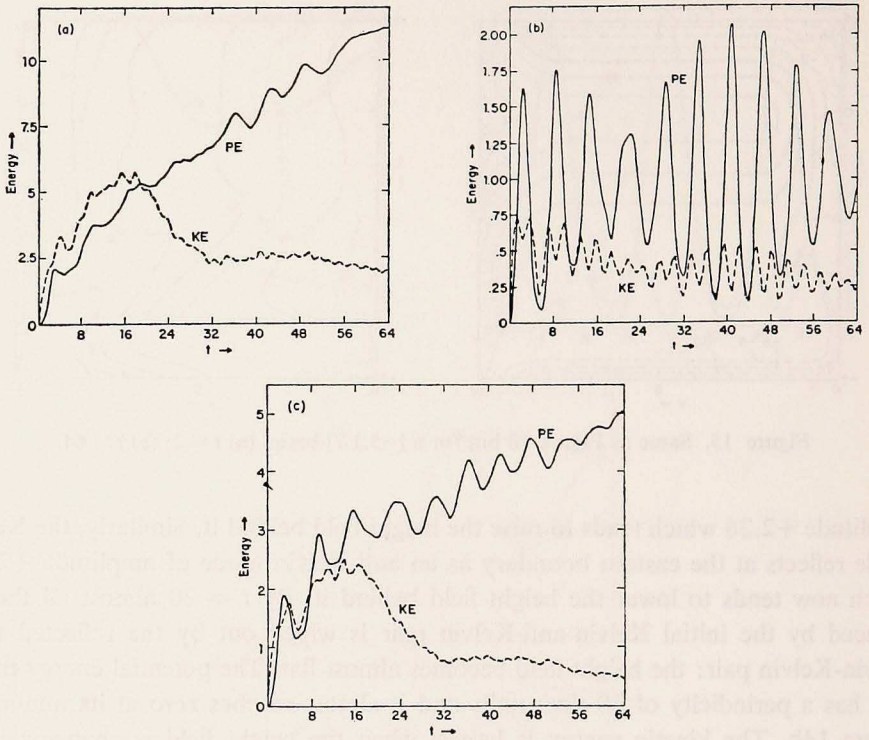

Figure 16. Energy versus time for the $G = 1$ case. (a) Basin [−5,5]; (b) Basin [−1.7,1.7]; (c) Basin [−5,1.7].

metry considerations, none of these modes contains any net meridionally integrated zonal mass flux, so that upon reaching the western boundary no Kelvin waves will ever be excited. According to Eq. (55), the zonally unbounded solution plus all its reflections sum simply to $(0,0,y)$, the final steady state. The response therefore proceeds relatively straightforwardly: the more Rossby waves emitted from the eastern boundary at $t = 0$ that reach a given point, the closer is the height field at the point to the final state. Thus points closer to the equator and to the eastern boundary spin up faster. The spin-up is monotonic with time—no Kelvin waves exist to slosh mass across the basin.

The response in the [−5,5] basin is very much the same as in the meridionally unbounded case except that the lowest planetary mode excited at the eastern boundary is now the $n = 0$ Rossby-Kelvin mode which does not exist in the meridionally unbounded case. Figure 16a shows the energy diagram for the [−5,5] basin. The wiggles, of period about 2π, are the initial $n = 0$ inertia-gravity waves (at $k = 0$, $\omega \cong 1$ in Fig. 1) which are excited initially to produce the zonally unbounded solution $(u^{(2)}, 0, h^{(2)})$ in Fig. 6a. Because the zonally unbounded state has a height field

which is tilted near the equator some moderate fraction of the final height field tilt and because this zonally unbounded state does not grow with time, the magnitude of the intertia-gravity oscillations are moderate and remain of constant amplitude. The initial $k = 0$, $\omega \cong 1$ has a group velocity to the east and reflects as a $k = -1$, $\omega \cong 1$ inertia-Kelvin wave—these reflections continue forever superimposed on the monotonically spinning-up height field.

Meridional sections of the height field in the [−5,5] case taken toward the end of the simulation ($t = 64$) indicate that the eastern part of the basin is almost completely spun up, as we expect, while the degree of spin-up at $t = 64$ decreases as we move westward across the basin. Because the $n = 0$ mode has its largest amplitude at the northern and southern walls (Fig. 4a) and travels with speed near unity, the regions near these walls are spun-up even at the west while substantial parts of the region between these walls and the equator have not yet felt the influence of any Rossby modes from the east and so are far from spun-up.

The energetics of the response in the [−1.7,1.7] case are shown in Figure 16b. In this case the inertia-gravity waves needed to set up the zonally unbounded solution have extremely large amplitude because the height field of this zonally unbounded solution (Fig. 6c) has a very substantial part of the tilt of the final spun-up height field. The envelope of the potential energy is modulated by the $n = 0$ inertia-gravity wave roundtrip transit time (calculated from the group velocities) which in the [−1.7,1.7] case is about 40 time units.

The asymmetric basin case, [−5,1.7], is completely different from the symmetric case in that the asymmetry of the basin modes now implies that *all* the modes carry net meridionally integrated zonal mass flux. Thus, in accordance with our discussion of western boundary response, Kelvin waves will be generated when any of the westward propagating modes reach the western boundary. Examining Table 2, we see that the zonally unbounded solution ($u^{(2)}$, 0, $h^{(2)}$) plus the reflections at the eastern boundary lead to a height field $h = y + .0986$ at the eastern boundary (by Eq. (55)), and by extension, to any point in the interior to which all the Rossby modes produced by this reflection have reached. The final steady state height field, however, is $h = y + 1.65$ so that even after all the Rossby modes due to the first reflection have reached all points, the tilt would be correct but there would still be a height deficit of 1.55 units throughout the basin. The additional mass, of course, is carried by the Kelvin wave which must reflect the total mass flux of the unbounded solution, −1.596. This Kelvin wave, of amplitude $b_K = 1.250$, thus carries a mass flux +1.596 and when at $t = 10$ (plus the wall-Kelvin travel time) this Kelvin mode hits the eastern boundary, it, plus its reflections, uniformly raises the height everywhere along the eastern boundary by an amount .979 according to Eq. (52) and Table 3. The initial Kelvin wave alone thus fills two-thirds of the height deficit. The initial anti-Kelvin, however, upon reflection at the western boundary, produces a Kelvin of negative amplitude −.786 which, when it hits the eastern boundary, lowers the

height field uniformly at the east by an amount .616, undoing some of the good works of the first Kelvin. From this point on, most of the mass flux in the succeeding reflections is sloshed around by the Kelvin mode reflecting into a Rossby-Kelvin mode and vice versa with a periodicity of 20 time units. Figure 16c shows the energy diagram for this case and we see that a plateau exists from $t = 20$ to 40 but that the inertia-gravity waves tend to mask the effect.

In order to filter out these inertia-gravity waves, we reran the $G = 1$, [−5,1.7] case starting, not from a flat ocean at rest, but rather from a state from which the inertia-gravity waves had already been removed, namely, the $(u^{(2)}, 0, h^{(2)})$ state. This filtering was largely successful and a comparable energy diagram shows that the 20 unit Rossby-Kelvin-Kelvin periodicity is clearly apparent. As time goes on, the height field would tilt closer to its final state, but contrary to the symmetric basin $G = 1$ cases, mass would continue to be sloshed across the basin.

6. Conclusion

This paper has presented a straightforward analytic approach to the calculation of the time-dependent response of equatorial basins to wind stresses varying slowly in the zonal direction and in time.[6] This allows (to our knowledge, for the first time) a rather detailed comparison of analytic theory with linear simulations, or equivalently, with the early (linear) stages of nonlinear simulations. The method involves first approximating and describing the free modes of a meridionally bounded basin; next calculating the meridionally bounded but zonally unbounded solution which gets set up by the emission of inertia-gravity waves within a single inertial period; then calculating the eastern and western boundary responses to this zonally unbounded solution and to any subsequent responses; and finally, following in time the series of reflections and responses that leads, or does not lead, to the steady state solution. The power of the method to accurately describe linear spin-up was illustrated by a series of numerical simulations of the responses of three separate ocean basins, [−5,5], [−5,1.7] and [−1.7,1.7], all 10 units long in the zonal direction, to the simple wind stress forcings $F = 1$ and $G = 1$, and following the response out to 64 nondimensional time units for each case.

Compared to the meridionally unbounded case treated in Paper II, we saw that the introduction of the northern and southern boundaries has in some ways simplified the consideration of spin-up and in some ways complicated it. For example, the problem is simpler in the $F = 1$ symmetric basin cases compared to the meridionally unbounded case in that only those modes whose turning points lie within the basin carry any meridionally integrated zonal mass flux, and all those modes whose turning points would have lain outside the basin in the meridionally unbounded case and which would have been needed to account for the rearrangement of mass dur-

6. Only winds independent of x and switched on in t were calculated explicitly but the extension to winds slowly varying in x and t is straightforward using the methods of Paper I.

ing spin-up are, in the symmetric basin case, replaced by a single anti-Kelvin mode. On the other hand, the problem is more complicated in these same cases in that the additional reflections induced by this same anti-Kelvin mode lead to a much more intricate reflection diagram (see Fig. 9). In the narrow basin case, [−1.7,1.7], the description becomes simpler still: since all Rossby modes higher than $n = 1$ have their turning points outside the basin, the complete system can be described by only three modes—the Kelvin, the anti-Kelvin and the $n = 1$ Rossby mode.

The results of the theory presented in Sections 2, 3, and 4, and of the simulations analyzed in Section 5, now allow us to address a question raised in the Introduction: to what extent does the imposition of the northern and southern boundaries affect the progress of the time-dependent response in the vicinity of the equator? The answer, as we saw, varies from case to case. The case in which the boundaries produced the least effect was the $G = 1$, [−5,5], case. Here the spin-up in the region of the equator was precisely the same as in the meridionally unbounded case. The only difference was that the fast $n = 0$ Rossby-Kelvin mode, with large amplitude at the northern and southern boundaries, spun up the regions near these boundaries rapidly, whereas this mode is totally absent in the unbounded case. In the $G = 1$, [−1.7,1.7], case, the boundaries are so close to the equator that the Rossby-Kelvin mode has considerable amplitude even at the equator. The entire basin would therefore spin-up relatively completely after only 10 time units (one Rossby-Kelvin mode traversal time) were it not for the large amplitude inertia-gravity waves set up during the initial unit of time. We can conclude that for $G = 1$, in basins symmetric with respect to the equator, the time-dependent response near the equator will proceed essentially unaffected by the northern and southern boundaries as long as these boundaries lie at least a few equatorial radii of deformation from the equator. For the $G = 1$ case, in basins asymmetric with respect to the equator, or for the $F = 1$ case in any of the basins, the extra Kelvin modes induced by the western boundary reflections of either anti-Kelvin or Rossby-Kelvin modes *will* change the details of the time-dependent response near the equator—the closer a boundary is to the equator the larger will be the change.

The role of the Kelvin mode in the spin-up process bears repeated comment. The *initial* Kelvin mode, in all those cases in which it exists ($G = 1$, asymmetric basin, and $F = 1$, all basins) helps to bring the height field closer to its spun-up (steady) value. On the other hand, repeated production of Kelvin modes by reflection of any of the westward propagating modes induces a sloshing of mass back and forth across the basin which inhibits the attainment of the final spun-up state. In the absence of friction, this sloshing would continue forever. Only in those cases in which the Kelvin mode never appears ($G = 1$, symmetric basins) does the time-dependent response truly proceed to a steady state.

It is clear that the method and results of this paper (and Papers I and II) are directly useful in analyzing numerical simulations of time-dependent response. But

in application to the real ocean we must offer a major *caveat*. We have assumed the existence of a single baroclinic mode. While there is evidence that standing vertical modes do exist (Wunsch and Gill, 1976), the question has recently been raised (Philander, 1978) of whether or not standing vertical modes are regularly excited by atmospheric forcing. Since the dynamics of baroclinic mode excitation is not at all well understood, we would urge the greatest caution in applying this, or any theory based on a single standing vertical mode, to the behavior of real oceans.

Acknowledgments. We would like to thank Brian Hickie for making available a copy of his paper prior to publication; Moshe Israeli for valuable help with the numerical work; Richard Lindzen for discussions of positive equivalent depth modes on β-planes; Dennis Moore and George Philander for continued discussions about the dynamics of equatorial waves; and D. R. Sadigur for careful preparation of the manuscript. This work was supported at Harvard University by NASA Grant NSG-5160.

APPENDIX: Orthogonality and completeness of the eigenfunctions

Fourier transforming the unforced ($F = G = Q = 0$) Eqs. (1) from x to k and denoting transpose by superscript T we may write (cf. I (36)ff):

$$\frac{\partial}{\partial t}(u,v,h)^T + i\,\mathbf{A}(u,v,h)^T = 0$$

where

$$\mathbf{A} \equiv \begin{bmatrix} 0 & iy & k \\ -iy & 0 & i\dfrac{\partial}{\partial y} \\ k & i\dfrac{\partial}{\partial y} & 0 \end{bmatrix}$$

then $\mathbf{A}\,\Phi_{n,j} = \omega_{n,j}\,\Phi_{n,j}$ and the following five lemmas follow easily:

Lemma 1 $\mathbf{A} = \mathbf{A}^*$ [Readily shown by direct calculation.]

Lemma 2 All the ω's are real. [Follows from the self-adjointness of $\mathbf{A}$, that is, from Lemma 1.]

Lemma 3 For all n, $\mu_n > 0$ [Since (1) and (2) form a standard Sturm-Liouville problem.]

Lemma 4 The ω's are distinct. [Follows from Lemma 3, the dispersion relation and a consideration of the Kelvin roots $\omega = \pm k$.]

Lemma 5 The $\{\Phi_{n,j}\}$ is orthogonal. [Follows from Lemma 4 in the usual way, i.e.

$$\omega_{m,l}\,[\Phi_{n,j}, \Phi_{m,l}] = [\Phi_{n,j}, \mathbf{A}\,\Phi_{m,l}] = [\mathbf{A}\,\Phi_{n,j}, \Phi_{m,l}] = \omega_{n,j}\,[\Phi_{n,j}, \Phi_{m,l}]$$

with the second equality a consequence of Lemma 1. Since the ω's are distinct, the Φ's are orthogonal.]

Theorem: $\{\Phi_{n,j}\}$ is complete.

Proof:

First rephrase the question of completeness as follows. Let $R = \{\Phi_{n,j} | n \geqslant 0\}$, i.e., all the eigenvectors except the Kelvin waves $\phi_{K,\pm 1}$. We wish to show that if

$$[(U, -iV, H)^*, \Phi_{n,j}] = 0 \text{ for all } \Phi_{n,j} \in R$$

then

$$V = 0;\ yH + U' = 0;\ \text{and } yU + H' = 0. \tag{A.1}$$

Since the only solutions to (A.1) are (multiples of) $\Phi_{K,\pm 1}$ the theorem will follow.

It is straightforward to show from the definition (37) of $\Phi_{n,j}$ that

$$[(U, -iV, H)^*, \Phi_{n,j}] = N_{n,j}^{-1} [A_{n,j}, \psi_n]$$

where

$$A_{n,j} = \omega_{n,j} (yU + H') + k(yH + U') + (\omega_{n,j}^2 - k^2) V .$$

Now by assumption

$$0 = [A_{n,j}, \psi_n] \text{ for all } j, n \geqslant 0 . \tag{A.2}$$

Hence

$$0 = [A_{n,j} - A_{n,l}, \psi_n] = (\omega_{n,j} - \omega_{n,l})[yU + H' + (\omega_{n,j} + \omega_{n,l}) V, \psi_n]$$

since

$$\omega_{n,j} \neq \omega_{n,l} \text{ for } j \neq l$$

$$(yU + H' + [\omega_{n,j} + \omega_{n,l}] V, \psi_n) = 0 \text{ for all } n \geqslant 0, j \neq l . \tag{A.3}$$

Let $l = 3$. Then taking the difference of (A.3) with $j = 1$ and $j = 2$ and using $\omega_{n,1} \neq \omega_{n,2}$ yields

$$(V, \psi_n) = 0 \text{ for all } n . \tag{A.4}$$

Since the ψ_n's are complete, $V = 0$. Then (A.3) implies that $yU + H' = 0$ and, finally, (A.2) yields $yH + U' = 0$, completing the proof.

In the body of this paper we make particular use of the completeness when $k = 0$. In this case the proof must be modified slightly. It is unchanged through (A.4) after which we must use

$$[(U, iV, H)^*, \Phi_{n,3}] = -(2\mu_n + 1)^{-1} (yU + H') + (yH + U')$$

to establish that

$$yH + U' = 0 .$$

REFERENCES

Abramowitz, M. and I. A. Stegun. 1965. Handbook of Mathematical Functions, New York, Dover, 1046 pp.

Anderson, D. L. T. and P. B. Rowlands. 1976. The role of inertia-gravity and planetary waves in the responses of a tropical ocean to the incidence of an equatorial Kelvin wave on a meridional boundary, J. Mar. Res., *34*, 295–312.

Cane, M. A. 1975. A study of the wind-driven ocean circulation in an equatorial basin. Ph.D. Thesis, Massachusetts Institute of Technology.

Cane, M. A. 1979. The response of an equatorial ocean to simple wind stress patterns: I. Model formulation and analytic results, J. Mar. Res., *37*, 233–252.

Cane, M. A. and E. S. Sarachik. 1976. Forced baroclinic ocean motions. I. The linear equatorial unbounded case. J. Mar. Res., *34*, 629–665.

Cane, M. A. and E. S. Sarachik. 1977. Forced baroclinic ocean motions. II. The linear equatorial bounded case. J. Mar. Res., *35*, 395–432.

Hickie, B. P. B. 1979. The effects of coastal geometry on equatorially trapped planetary waves. Part I: Free oscillations in the Gulf of Guinea. To appear.

Matsuno, T. 1966. Quasi-geostrophic motions in the equatorial area. J. Met. Soc. Japan, *44*, 25–43.

Mofjeld, H. O. and M. Rattray, Jr. 1971. Free oscillations in a beta-plane ocean. J. Mar. Res., *29*, 281–305.

Moore, D. W. 1968. Planetary-gravity waves in an equatorial ocean. Ph.D. Thesis, Harvard University.

Moore, D. W. and S. G. H. Philander. 1976. Modelling of the tropical oceanic circulation, *in* The Sea, Vol. 6, Chapter 8, Goldberg *et al.*, eds., New York, Interscience, 1048 pp.

Philander, S. G. H. 1978. Forced oceanic waves. Revs. Geophys. Space Phys., *16,* 15–46.

Wunsch, C. and A. E. Gill. 1976. Observations of equatorially trapped waves in Pacific sea level variations. Deep Sea Res., *23,* 371–390.

Received: *18 August, 1978;* revised: *3 March, 1979.*